

# SORPTION OF CARBON DIOXIDE BY COALS

John W. Larsen

The Energy Institute  
Coal Utilization Laboratory  
The Pennsylvania State University  
University Park, PA 16802

## Introduction.

When CO<sub>2</sub> is adsorbed on the surface of a coal, two equilibria are established. One is between adsorbed CO<sub>2</sub> and gas phase CO<sub>2</sub>. The other is between adsorbed CO<sub>2</sub> and CO<sub>2</sub> dissolved in the coal. Pressure has a significant effect on both equilibria. In this paper, the sorption of CO<sub>2</sub> by coals will be considered in the light of these simultaneous equilibria. When the coal-CO<sub>2</sub> system is at equilibrium, CO<sub>2</sub> in the gas phase, on the coal surface, and dissolved in the coal will all have the same activity. The time required to dissolve CO<sub>2</sub> in coals and establish equilibrium may be long.

## Results and Discussion.

Adsorption thermodynamics. It is difficult to measure the thermodynamics of adsorption of CO<sub>2</sub> on a coal. The problem is separating the two equilibria. Static techniques, such as those routinely used for BET surface area measurements, measure total CO<sub>2</sub> uptake by the coal, both surface CO<sub>2</sub> and dissolved CO<sub>2</sub>. The resulting thermodynamic quantities are for some mixture of the two equilibria, the mixture depending on the pressure and the diffusion rate of the CO<sub>2</sub> into the coal.

Gas chromatography using coal packed columns (inverse GC) has been used to measure the isosteric heads of adsorption of CO<sub>2</sub> and other gasses on Illinois No. 6 coal.<sup>1,2</sup> This is a transient technique that does not allow time for the CO<sub>2</sub> to diffuse into the coal so only one equilibrium is established.<sup>1</sup> The isosteric enthalpy of CO<sub>2</sub> adsorption on Illinois No. 6 coal is -6.6 kcal/mole. Of this, London dispersion interactions are responsible for -2.5 kcal/mole and polar interactions are responsible for the rest. This enthalpy is greater than the corresponding value for methane (-3.1 kcal/mole) and about the same as for ethane (-6.4 kcal/mole).<sup>2</sup>

Coal surface areas measured by CO<sub>2</sub> adsorption. With two equilibria involved in static measurements, are the numerous coal surface areas that have been measured using CO<sub>2</sub> adsorption correct? I believe that they are approximately correct and still very useful. This belief is based in part on the agreement between surface areas measured by CO<sub>2</sub> adsorption and other techniques, such as X-Ray scattering.<sup>3</sup> Also, as pointed out by Walker and Mahajan, surface areas are measured by using very low CO<sub>2</sub> pressures and the amount of CO<sub>2</sub> dissolved under these conditions is usually too small to vitiate the surface area measurements.<sup>4</sup> As will be seen, the results for bituminous coals are more reliable than those for low rank coals.

Table 1 contains the surface areas of the Argonne Premium Coals measured by CO<sub>2</sub> and ethane (C<sub>2</sub>H<sub>6</sub>) using the standard static BET technique at -78 °C.<sup>5</sup> Ethane and CO<sub>2</sub> have similar cross sectional areas, 25.3 Å<sup>2</sup> and 25.1 Å<sup>2</sup> respectively. The surface areas measured using CO<sub>2</sub> are much larger, as much as 25 times larger, despite the gasses being of similar size and shape and the measurements being made at the same temperature. There are three possible explanations. 1) The pore structure of all of these coals is so finely tuned that it allows passage of CO<sub>2</sub> while not allowing ethane to pass. 2) The CO<sub>2</sub> is dissolving in the coals while ethane is not. 3) CO<sub>2</sub> diffuses rapidly through the coals while ethane diffusion is slow.

Explanation 1 is not reasonable. The molecules are of such similar size and shape that the necessary level of discrimination by a

rigid pore system is most unlikely. That 8 pore systems should be so finely discriminatory is unreasonable. The only problem with explanation two is that CO<sub>2</sub> adsorption does give coal surface areas in agreement with other techniques. If this is generally correct (and it deserves more testing), then the CO<sub>2</sub> is not dissolving in the coal in large amounts. Explanation three is preferred. Stated again in more detail: CO<sub>2</sub>, because it interacts with coals in ways that ethane cannot, has some solubility in coals and diffuses rapidly through them to reach all of the pore surfaces where it is adsorbed. If this is the correct explanation, then ethane diffusivity through coals must be slow. It has been measured only for Illinois No. 6 coal. Ethane uptake was not complete in 131 hr. While I prefer explanation 3, uncertainty remains. The diffusivities of gasses through coals and diffusion mechanisms deserve more study.

**Table 1. BET Surface Areas (m<sup>2</sup>/g) of the Argonne Coals Measured at -78 °C Using CO<sub>2</sub> or Ethane (data from ref. 5)**

| Coal (%C, dmmf)       | CO <sub>2</sub> | Ethane |
|-----------------------|-----------------|--------|
| Pocahontas (92)       | 202             | 69     |
| Upper Freeport (88)   | 166             | 72     |
| Stockton (85)         | 175             | 34     |
| Pittsburgh No. 8 (85) | 177             | 37     |
| Blind Canyon (81)     | 239             | 122    |
| Illinois No. 6 (81)   | 132             | 38     |
| Wyodak (76)           | 330             | 106    |
| Beulah Zap (74)       | 274             | 11     |

Dissolution of CO<sub>2</sub> in coals. In order to understand the dissolution of CO<sub>2</sub> in coals, some background on the physical structure of coals is needed. Coals are strained glassy materials prevented from rearranging into their most stable physical structure by non-covalent interactions too strong to be overcome by thermal energy.<sup>6</sup> When substances dissolve in coals, the glass to rubber transition temperature (T<sub>g</sub>) is lowered. Even small amounts of material, for example toluene adsorbed from the vapor state, suffice to enable the coal structure rearrangement.<sup>7</sup> The rearrangement has been characterized and proceeds to a more highly associated structure in which fluids are significantly less soluble.<sup>6</sup> Organic molecules dissolved in coals can be efficient plasticizers that enable physical structure rearrangements. They also lower the softening temperature of coals and can lead to flexible rubbery systems.<sup>8</sup>

It was known as early as the 1930s that CO<sub>2</sub> dissolved in coals, swelling them.<sup>9</sup> But it was not until 50 years later that it was suggested that CO<sub>2</sub> dissolution had an invidious effect on surface areas measured by CO<sub>2</sub> adsorption.<sup>10,11</sup> The pressure of CO<sub>2</sub> used, the volumetric swelling of the coal, and the % of the CO<sub>2</sub> that is dissolved are given in Table 2.

**Table 2. Carbon Dioxide Adsorption and Dissolution (data from ref. 11)**

| Coal (% C, daf) | Pressure (atm) | Swelling Vol. % | % CO <sub>2</sub> Dissolved |
|-----------------|----------------|-----------------|-----------------------------|
| KCER 7259 (84)  | 5              | 0.75            | 14                          |
|                 | 10             | 0.85            | 16                          |
|                 | 15             | 1.33            | 24                          |
| KCER 7122 (78)  | 5              | 1.24            | 23                          |
|                 | 10             | 2.23            | 41                          |
|                 | 15             | 3.11            | 58                          |
| KCER 7463 (66)  | 5              | 2.16            | 24                          |
|                 | 10             | 3.00            | 33                          |
|                 | 15             | 4.18            | 47                          |

As expected, the amount of CO<sub>2</sub> absorbed by the coals increases with pressure as does the % of CO<sub>2</sub> that is dissolved. This is the expected effect of increases in CO<sub>2</sub> fugacity and further pressure increases will lead to greater CO<sub>2</sub> dissolution and increased swelling. The amount of CO<sub>2</sub> dissolved increases with decreasing coal rank as expected if polar interactions are important. With increasing pressure, the rates of coal swelling increase. For example, the time to reach half of the maximum swelling of the 84% C coal decreases from about 40 hr at 1 atm to about 10 hr at 15 atm. It is clear from these data that CO<sub>2</sub> readily dissolves in coals, swelling them. The initial swelling by CO<sub>2</sub> is anisotropic, just as it is with organic liquids.<sup>12, 6</sup> It is expected to act as a plasticizer enabling the coals to rearrange at some (probably slow) rate and lowering their softening temperatures. A crucial question for CO<sub>2</sub> sequestration in coals is "how good a plasticizer is CO<sub>2</sub>?"

There are very few data that bear on this question. Figure 1 shows the effects of CO<sub>2</sub> and He at elevated pressures on the softening temperature of a high rank Lower Kitaning coal (PSOC 1197, 91 %C, dmmf).<sup>13, 14</sup> As expected, He has no effect on the coal's softening temperature. The data for CO<sub>2</sub> are stunning. The coal softening temperature begins to drop sharply at a CO<sub>2</sub> pressure of 30 atm and has dropped to about 300 °K at 55 atm CO<sub>2</sub> pressure. This is a 373°C decrease in softening temperature. In this coal, CO<sub>2</sub> is a very effective plasticizer. It will efficiently enable coal structure rearrangements; these rearrangements are known to decrease the solubility of organic liquids in coals and I expect the rearrangement will have the same effect on CO<sub>2</sub> solubility and strongly decrease it. If these results are general, pumping high pressure CO<sub>2</sub> into coal seams will readily dissolve the CO<sub>2</sub> in the coals. This may enable structure rearrangements that will decrease CO<sub>2</sub> solubility forcing some of the dissolved CO<sub>2</sub> back out of the coal. Pressure will increase T<sub>g</sub> and tend to keep the coal from rearranging. The rates of the possible coal rearrangement as a function of CO<sub>2</sub> pressure, temperature, and lithostatic pressure on the coal are not known. The effect of structure rearrangements on CO<sub>2</sub> solubility in coals is not known. This information is crucial to understanding and evaluating the possibility of sequestering CO<sub>2</sub> in coal seams for geological time periods.

**Acknowledgement.** My work in this area over the years has been supported by the U. S. Department of Energy to whom I am grateful.

## References

- (1) Glass, A. S.; Larsen, J. W. *Energy Fuels* **1994**, *8*, 629-636.
- (2) Glass, A. S.; Larsen, J. W. *Energy Fuels* **1993**, *7*, 994-1000.
- (3) Spitzer, Z.; Ulicky, L. *Fuel* **1977**, *55*, 212-224. Gethner, J. S. *J. Appl. Phys.* **1986**, *59*, 1068-1085.
- (4) Walker, P. L. Jr.; Verma, S. K.; Rivera-Utrilla, J.; Khan, M. R. *Fuel* **1988**, *67*, 719-726.
- (5) Larsen, J. W.; Hall, P.; Wernett, P. C. *Energy Fuels* **1995**, *9*, 324-330.
- (6) Larsen, J. W.; Flowers, R. A. II; Hall, P.; Carlson, G. *Energy Fuels* **1997**, *11*, 998-1002.
- (7) Hsieh, S. T.; Duda, J. L. *Fuel* **1987**, *66*, 170-178.
- (8) Yang, X.; Silbernagel, B. G.; Larsen, J. W. *Energy Fuels* **1994**, *8*, 266-275.
- (9) Briggs, H.; Sinha, R. P. *Proc. Roy. Soc. Edinburgh* **1933**, *53*, 48
- (10) Reucroft, P.J.; Patel, K. B. *Fuel* **1983**, *62*, 279.
- (11) Reucroft, P. J.; Sethuraman A. R. *Energy Fuels* **1987**, *1*, 72-75.
- (12) Ceglarska-Stefanska, G.; Czaplinski, A. *Fuel* **1993**, *72*, 413-417.
- (13) Khan, M. R.; Jenkins, R. G. *Proc. Int. Conf. Coal Sci.* **1995**,
- (14) Khan, M. R. Ph.D. Thesis, The Pennsylvania State Univ. **1985**.

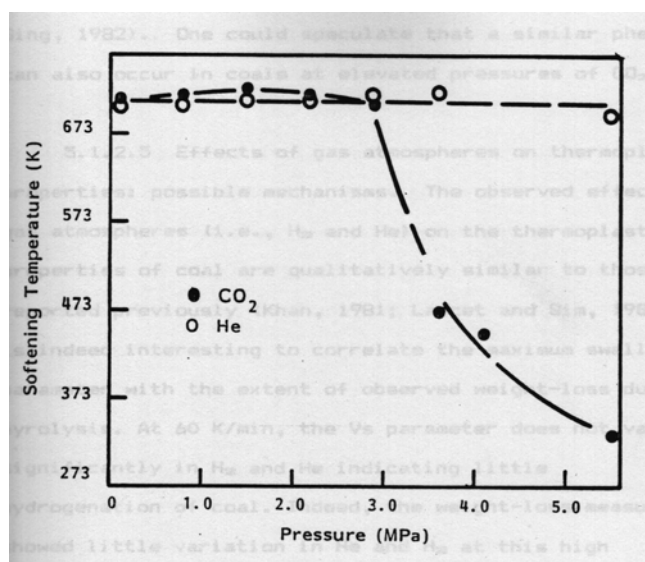


**Figure 1.** The Effect of He and CO<sub>2</sub> on the Softening Temperature of a Lower Kitaning (91% C, dmmf) Coal (from ref. 13)

# AN INITIAL SET OF WORKING HYPOTHESES CONCERNING SOME CHEMICAL AND PHYSICAL EVENTS WHEN CO<sub>2</sub> IS INJECTED INTO A COALBED

CURT M. WHITE

National Energy Technology Laboratory  
P. O. Box 10940  
Pittsburgh, PA 15236

In any new area of science it is often beneficial to formulate hypotheses and then work toward proving, disproving and refining them. Such is the case with sequestration of CO<sub>2</sub> in coal seams with concomitant recovery of methane. This is a new technology that has been practiced in a few places but is not well developed. Off-the-shelf technology is available to perform CO<sub>2</sub>-enhanced coalbed methane recovery/sequestration (CO<sub>2</sub>-ECBM/sequestration). Burlington Resources performed CO<sub>2</sub>-ECBM in deep unmineable coal seams in the San Juan Basin in New Mexico in 1996.<sup>1</sup> Very little information has entered the public domain from this or similar projects. There is a very incomplete understanding of what happens when CO<sub>2</sub> is injected into a coal seam. During the preparation of a review article on CO<sub>2</sub>-ECBM/sequestration we formulated a number of hypotheses concerning the chemical and physical phenomena that occur when CO<sub>2</sub> is injected into a coal seam. Information gathered from the literature was combined with our knowledge of both the chemical and physical properties of coal and supercritical CO<sub>2</sub> to yield a set of working hypotheses that begin to describe the process.

## Hypotheses

- 1) The glass-to-rubber transition temperature ( $T_g$ ) of the coal will be dramatically reduced by imbibition of CO<sub>2</sub>. The coal will become plasticized.<sup>2</sup>
- 2) The cleat system within the coalbed will begin to close and become restricted, slowing Darcy flow within that area of the seam due to swelling.
- 3) There will be a substantial increase in the self diffusivity of CO<sub>2</sub> in coal once it has become plasticized and is above its  $T_g$ .<sup>2</sup>
- 4) The diffusivity of CO<sub>2</sub> in coal swollen by high pressure CO<sub>2</sub> can be described by free volume theory.
- 5) Both liquid and supercritical CO<sub>2</sub> will extract small molecules trapped within the coal macromolecular network. As the network relaxes, these molecules will be released and move with the CO<sub>2</sub> as long as the pressure is above their threshold pressure.
- 6) Some of the minerals commonly found in coal will dissolve in the acidic, carbonated water during those times when both water and CO<sub>2</sub> are present together in the coal.
- 7) The Ca and Mg content of the coal will decrease due to dissolution of carbonate minerals by carbonic acid and to due Ca and Mg being displaced from carboxylic acids in low rank coal.
- 8) Injection of CO<sub>2</sub> will dry the coal, particularly in those areas where the flow rate of CO<sub>2</sub> is highest.
- 9) There will be a CO<sub>2</sub> pressure gradient across the coalbed. When dissolved minerals and organics reach areas of the seam with lower pressure they will precipitate causing the seam to begin to clog the coal's pores.

## Discussion

**Effect on Diffusivity** The plasticization effects of CO<sub>2</sub> on coal (hypotheses 1 and 4) are discussed elsewhere.<sup>2</sup> Hypothesis 4 is an extension of one proposed by Larsen to include the self diffusion of CO<sub>2</sub> in plasticized coal. Mass transport through coal is a controlling function in the sequestration of CO<sub>2</sub> in coal. If the cleat fracture system in a coal becomes restricted due to swelling, then Darcy flow will be restricted and transport through the coal will be primarily Fickian and possibly Knudsen.

A substantial increase in molecular diffusivity of guest molecules in macromolecular systems in contact with supercritical CO<sub>2</sub> has been documented recently. For example, the diffusivity of ethylbenzene in CO<sub>2</sub> swollen polystyrene shows a 10<sup>6</sup> fold increase when supercritical CO<sub>2</sub> is present.<sup>3</sup> Experimental information that defines factors that impact and control transport properties in CO<sub>2</sub> swollen macromolecular systems is limited for polymeric systems and to our knowledge, unknown for coals. The transport properties of Co(II) complexes in polymeric systems in contact with supercritical CO<sub>2</sub> are dependent upon the degree of CO<sub>2</sub> swelling and the degree of plasticization.<sup>4</sup> These are plasticization induced changes in the transport properties of guest molecules in the swollen macromolecular network. We hypothesize that the substantial increases in diffusivity of guest molecules in polymeric systems applies to the self diffusion of CO<sub>2</sub> in CO<sub>2</sub> swollen macromolecular systems such as coal. As such, we expect diffusion of CO<sub>2</sub> in coal swollen by high pressure supercritical CO<sub>2</sub> will be much more rapid than in the same coal before plasticization.

What is the diffusivity of CO<sub>2</sub> in coal swollen by high pressure supercritical CO<sub>2</sub>? Lee *et al.*<sup>4</sup> recently showed that in a polymeric system swollen by CO<sub>2</sub>, the effect of CO<sub>2</sub> swelling on mass transport is related to free volume theory.

They estimated the fractional free volume (FFV) of swollen polymeric system from the following relationship:

$$FFV = \frac{V_m - V_w}{V_m}$$

where  $V_m = M/d$  is the molar volume of the swollen polymer,  $M$  and  $d$  are the molecular weight and density of the swollen polymer, and  $V_w$  is the estimated van der Waals volume. CO<sub>2</sub> diffusivity should decrease exponentially with the reciprocal free volume,  $1/FFV$ . As swelling increases, free volume increases and diffusivity increases. We strongly suspect that the same theoretical approach will explain CO<sub>2</sub> diffusion in supercritical CO<sub>2</sub> swollen coals, and allow estimation of the CO<sub>2</sub> diffusivity under a variety of conditions in swollen coal matrices.

**Effect Of CO<sub>2</sub> Adsorption On Organic Matter** When CO<sub>2</sub> interacts with coal, multiple processes occur. CH<sub>4</sub> sorbed onto coal is displaced by CO<sub>2</sub>. CH<sub>4</sub> desorption occurs simultaneously with CO<sub>2</sub> adsorption. CH<sub>4</sub> is displaced into the cleat system of the coal where it begins to move toward an area of lower pressure, the production well. CH<sub>4</sub> desorption causes coal to shrink, whereas CO<sub>2</sub> adsorption causes the coal to swell. In general, coal swelling due to CO<sub>2</sub> sorption is greater than shrinkage caused by CH<sub>4</sub> desorption. The net effect is coal swelling. As CO<sub>2</sub> is imbibed by coal, the coal swells causing the

macromolecular structure to relax.<sup>2</sup> Weak intermolecular interactions such as van der Waals interactions, hydrogen bonds and charge transfer interactions between one part of the macromolecule and another or between two macromolecules are broken and replaced by interactions between the macromolecule and CO<sub>2</sub> molecules. This allows the small molecules trapped within the interwoven macromolecular network to be released, so that they are free to move. Liquid and dense gaseous CO<sub>2</sub> are excellent solvents. As the trapped molecules are released, they become solvated and extracted by the CO<sub>2</sub>, and migrate with CO<sub>2</sub> throughout the coalbed. The extraction process and movement of formerly trapped molecules begins with the lower molecular weight compounds first. Movement of compounds is a function of each compound's threshold pressure. The threshold pressure of a substance was originally defined by Giddings as the lowest supercritical pressure that will cause a substance to just begin migrating in a flowing stream of supercritical fluid.<sup>5</sup> Among hydrocarbons the threshold pressure is an approximate function of their molecular weight. Generally, the amount extracted from coal is quite small, about 2.5 weight percent or less.

**Effect Of CO<sub>2</sub> Adsorption On Mineral Matter** The presence of high pressure CO<sub>2</sub> and water can also have a profound effect on the mineral matter present in coal. Many minerals present in coal are soluble in acidic aqueous solutions. The solubility of CO<sub>2</sub> in water is substantial at high pressures. According to simulations we performed, the pH of aqueous CO<sub>2</sub> solutions at 300 atm and 45°C is less than 3.0. The alkaline earth metals are removed from coal by treatment with acidic aqueous solutions. Calcite, dolomite, and other carbonate minerals are removed from coal at room temperature by extraction under acidic conditions with aqueous CO<sub>2</sub> solutions. Hayashi *et al.* studied the removal of Ca and Mg from several low rank coals by batch extraction with CO<sub>2</sub> dissolved in water at 600 kPa and 25°C at various extraction times.<sup>6</sup> They showed that the Ca removal yield is affected by the total Ca content of the coal and the total carboxyl content. Ca removal is also affected by the coal:water ratio in that Ca removal decreases as the amount of water decreases. During CO<sub>2</sub> sequestration in coal, it is expected that the water content of the coal will initially decrease with time. The coal will most probably be dewatered before CO<sub>2</sub> injection begins. This process will remove some of the bulk water in the cleat system. When CO<sub>2</sub> injection begins, we expect that the remaining water in the cleat system will be reduced further and the water present in the pores will also be reduced. The rate and extent of these processes are unknown. Thus, we expect that initially the Ca and Mg content of the coal will be reduced when both water and CO<sub>2</sub> are present. The dissolved minerals will be transported through the coal seam and eventually recovered in the produced water when the process is taken to completion. As the water content decreases, the amount of Ca and Mg removed will decrease. If water migrates back into the seam, then Ca and Mg removal could increase. The solubility of carbonate minerals in acidic aqueous solutions is dependent upon both H<sub>2</sub>O and CO<sub>2</sub> being present.

**Drying of Coal by Flowing CO<sub>2</sub>** Iwai *et al.* report the use of supercritical CO<sub>2</sub> to dry coal.<sup>7</sup> Water could be removed by either becoming solubilized by the CO<sub>2</sub> or by being displaced by it. Water is only sparingly soluble in supercritical CO<sub>2</sub>. Under some conditions water is almost quantitatively removed from low rank coals. They showed that drying of ground and sieved coal (8

grams, 18-30 mesh) with CO<sub>2</sub> (1.5 moles/hour for 20 hours) at either 9.8 or 14.7 MPa and 40°C resulted in removal of water and increased both the surface area and the pore volume of the coal. The degree of coal drying that will occur during CO<sub>2</sub>-ECBM/sequestration is unknown, but will probably not be quantitative except near the injection well. Water that is removed during the dewatering process and that removed by CO<sub>2</sub> can be continually replaced by recharge of water from the aquifers.

**Precipitation Due to the Pressure Drop** There will be both a pressure drop and a CO<sub>2</sub> partial pressure drop from the point of injection to the production well. The injected CO<sub>2</sub> follows the path of least resistance, moving from areas of high pressure near the injection well to those of lower pressure (toward the production well) through the areas of the coalbed that have the highest permeability. As injection continues, the areas of highest permeability become less permeable with time because the swelling process begins to close the cleat system which initially controls gas transport within the coalbed. The extracted compounds that are moving with the flowing CO<sub>2</sub> will begin to clog or plug the coal's pores.<sup>8</sup> The effect of this pore clogging on permeability is unknown. The back pressure increases due to closing of the cleat system caused by swelling. The CO<sub>2</sub> begins to flow into other areas of the coalbed that now represent areas of higher permeability. Eventually, many areas of the cleat system begin to swell. When this happens, the pressure across the coalbed begins to rise, increasing the density and solvating power of the CO<sub>2</sub>. The precipitated components then begin to redissolve according to their threshold pressure. As the redissolution process occurs, flow begins again from areas of high pressure toward the production well. The CO<sub>2</sub> will move through the coal as a front, similar to frontal chromatography. The partial pressure of CO<sub>2</sub> will be high in areas behind the front and at the front, but low ahead of the moving CO<sub>2</sub> front. When dissolved carbonate minerals migrate to areas of lower CO<sub>2</sub> partial pressure and/or decreased amounts of water they will precipitate out of solution.

Eventually, the flowing CO<sub>2</sub> finds its way to the area of lowest pressure at the production well. The pressure decreases as CO<sub>2</sub> nears the production well, causing the CO<sub>2</sub> density and solvent strength to decrease. This in turn will cause the organic molecules extracted by the CO<sub>2</sub> and the dissolved minerals to precipitate again when the pressure becomes less than their threshold pressure, clogging the coal matrix adjacent to the production well. Eventually, these molecules will be re-extracted as the CO<sub>2</sub> pressure builds up behind them, redissolving them and moving them into the production well. These are only initial hypotheses that await additional experimental confirmation from the lab and field.

## References

- (1) Stevens, S. H.; Kuuskraa, V. A.; Spector, D.; Riemer, P. *CO<sub>2</sub> Sequestration in Deep Coal Seams: Pilot Results and Worldwide Potential*, IEA Greenhouse Gas R&D Programme 1999.
- (2) Larsen, J. W. *Polymeric Nature of Coals: Some Consequences and Some Unknowns*, ICCS, San Francisco, 2001.
- (3) Dooley, K. M.; Launey, D.; Becnel, J. M.; Caines, T. L. *Measurement and Modeling of Supercritical Fluid Extraction from*

Polymeric Matrices, 1995, *ACS Symp. Series 608*, Chapter 18, 269.

(4) Lee, D.; Hutchison, J. C.; Leone, A. M.; DeSimone, J. M.; Murray, R. *W. J. Am. Chem. Soc.* **2002**, *124*, 9310.

(5) Giddings, J. C.; Myers, M. N.; King, J. W. *J. Chromatographic Sci* **1969**, *7*, 276.

(6) Hayashi, J.; Hayashi, K.; Takeuchi, K.; Kusakabe, S. Morooka, *Fuel* **1991**, *70*, 1181.

(7) Iwai, Y.; Murozono, T.; Koujina, Y.; Arai, Y.; Sakanishi, K. *J.*

*Supercritical Fluid* **2000**, *18*, 73.

(8) Levine, J. R. *Proceedings of the 1991 Coalbed Methane Symposium*, 307.

# MECHANISM OF CARBON DIOXIDE (CO<sub>2</sub>) ADSORPTION ON MOIST COALS

Ekrem Ozdemir,<sup>1,2</sup> Karl Schroeder,<sup>1</sup> Badie I. Morsi<sup>1,2</sup>  
and Curt M. White<sup>1</sup>

<sup>1</sup> U.S. Department of Energy - National Energy Technology  
Laboratory (NETL), P.O.Box 10940, Pittsburgh, PA 15236

<sup>2</sup> Chemical and Petroleum Engineering Department, University of  
Pittsburgh, 1249 Benedum Hall, Pittsburgh, PA 15261

## Introduction

Sequestration of carbon dioxide (CO<sub>2</sub>) in coal seams is being considered as a strategy for mitigating green house gas emissions. The adsorption of CO<sub>2</sub> onto a solid, immobile matrix that will be stable over geologic times is considered an important advantage of coal seam sequestration. However, the adsorption capacity and the stability of the adsorbed CO<sub>2</sub> are affected by the nature of the coal and the environment in which it is placed. Pressure, temperature, coal rank, coal moisture content, and changes in the pH of the coalbed water are factors that may limit the extent of adsorption.<sup>1</sup> Because it is well recognized that the methane adsorption capacity of coal decreases with increasing moisture content, the effect of moisture on the CO<sub>2</sub> adsorption capacity is of special interest.<sup>2,3</sup> To our knowledge, there is no systematic study of the effect of moisture on the adsorption isotherm and adsorption capacity of CO<sub>2</sub> on coals.

The adsorption mechanism in microporous adsorbents has been interpreted in terms of both a pore filling process, using the Dubinin pore filling equation, and a surface adsorption, using the Langmuir or BET equation.<sup>4</sup> Martinez *et al.*<sup>5</sup> studied the mechanism of adsorption of CO<sub>2</sub> on activated anthracite and concluded that the adsorption mechanism was dependent on the shape and size of the pores. They suggested that the adsorption was a pore filling process in narrow micropores of molecular dimensions and gave rise to the curvature seen at lower pressures in the adsorption isotherm. Adsorption in wider pores was dominated by surface adsorption that produced an isotherm with a rectilinear shape. Levy *et al.*<sup>6</sup> showed that the adsorption capacity of CH<sub>4</sub> on coals increased linearly from 12 ml/g to 26 ml/g as moisture decreased from 4% to 0.5%. While it is tempting to interpret some of the isotherm data as a simple competition between moisture and adsorbing gas (CH<sub>4</sub> or CO<sub>2</sub>), it is recognized that moisture can play a role in the 3-dimensional structure of the organic coal matrix. Suuberg *et al.*<sup>7</sup> showed that coals shrink when dried. A plot comparing the volumetric shrinkage to the percent moisture loss was linear for a dozen coals of different ranks. For the lower rank coals, the volumetric shrinkage amounted to 25-30%. They pointed out that the measurement of the surface areas of dried coals might provide an erroneous estimate of the true accessibility of the coal structure.

## Experimental

**Moisture content.** In order to obtain coal samples with various moisture contents, as-received samples of Argonne coals<sup>8</sup> were dried *in-situ* in the adsorption apparatus. Each of the samples was vacuum-dried individually at 22, 22, 45, 80, or 97°C for 4, 20, 10, 16, or 5 hrs, respectively. After drying, the coals were allowed to equilibrate at the temperature and pressure of the initial isotherm experiment for 2-3 hrs before beginning the adsorption isotherm measurements. After the adsorption experiments, the moisture content of each of the samples was determined using Thermal Gravimetric Analysis (TGA). TGA drying experiments were conducted on 23 mg samples, at 105 °C for 60 min.

**Evaluation of adsorption isotherm data.** Gaseous CO<sub>2</sub> adsorption isotherms were obtained by the volumetric method using a low-sample-volume apparatus described elsewhere.<sup>9</sup> The isotherms were evaluated using an equation derived previously (Eq.1) that attempts to account for the volumetric swelling of the coal.<sup>9</sup>

$$n^{ex} = n^{abs} + \left(\frac{\Delta V}{RT}\right) \left(\frac{P}{z}\right) \quad (1)$$

The absolute amount adsorbed,  $n^{abs}$ , can be represented by the Langmuir or Dubinin-Astakhov equations which assume surface coverage or pore filling mechanisms, respectively. In the case of the pore filling mechanism, Eq.1 becomes Eq.2, which accounts for the volume of the adsorbed phase:

$$n^{ex} = \left(1 - \frac{\rho}{\rho^a}\right) n_0 e^{-D \left[\ln\left(\frac{P_s}{P}\right)\right]^j} - \rho \Delta V_c \quad (2)$$

where  $n^{ex}$  is the experimentally determined adsorption (Gibbs adsorption),  $\rho$  is the density of the adsorbing gas,  $\rho^a$  is the density of the adsorbed phase,  $n_0$  is the adsorption capacity,  $P_s$  is the saturation pressure,  $\Delta V_c$  is the change in the accessible pore volume,  $j$  is the Dubinin exponent related to the pore size distribution, and  $D$  is Dubinin constant defined as

$$D = \frac{RT}{\beta E_0} \quad (3)$$

where  $R$  is the universal gas constant,  $T$  is temperature,  $\beta$  is the affinity coefficient, and  $E_0$  is the characteristic heat of adsorption.

## Results and Discussion

**Figure 1** shows the adsorption isotherms of CO<sub>2</sub> on four of the eight Argonne Premium coals. These are representative of the different ranks and moisture contents of the coals. Pocahontas No.3 was the highest rank coal and contained the least moisture (0.63%). Pittsburgh No.8, Blind Canyon, and Wyodak coals decrease in rank and increase in moisture content, successively. Drying the coals at 80 °C for 20 hrs under vacuum removed a smaller fraction of the total moisture content for the higher rank coals and a progressively larger fraction for the lower rank coals. For instance, the moisture content decreased from 0.63% to 0.54% (14% of the initial moisture was removed) for Pocahontas No.3, a high rank coal, but decreased from 20.72% to 3.40% (84% removed) for the low rank Wyodak coal.

The effect of moisture removal was smaller for the higher rank coals than for the lower rank coals. The CO<sub>2</sub> adsorption isotherm for the high rank Pocahontas No.3 changed little, but the original moisture content was small. On the other hand, significant increases in adsorption were seen for the dried low-rank coals.

The amount of CO<sub>2</sub> adsorbed on a particular coal was determined from the adsorption isotherm and was found to be directly related to the moisture content of the coal. **Figure 2** shows the adsorption isotherms of CO<sub>2</sub> on the Argonne Premium Illinois No.6 coal dried to different moisture contents. The apparent amount of CO<sub>2</sub> adsorbed ( $n^{ex}$ ) increased as more and more moisture was removed from the as-received coal. The shapes of the adsorption isotherms for the as-received (moist) coals were Langmuir-like whereas the adsorption isotherms for the dried coals were more rectilinear.

**Figure 3** shows the adsorption capacity of the eight Argonne Premium coals dried to different moisture contents. The adsorption capacity is linearly related to the moisture content of each coal, regardless of rank. This trend is similar to that observed by Suuberg<sup>7</sup> for volumetric shrinkage (*vide supra*) and we believe the two are related. The adsorption capacities of the dried coals calculated from the intercepts in **Figure 3** were found to be rank dependent. Thus, the

extent of adsorption of CO<sub>2</sub> on a given coal is dependent on its rank and moisture content.

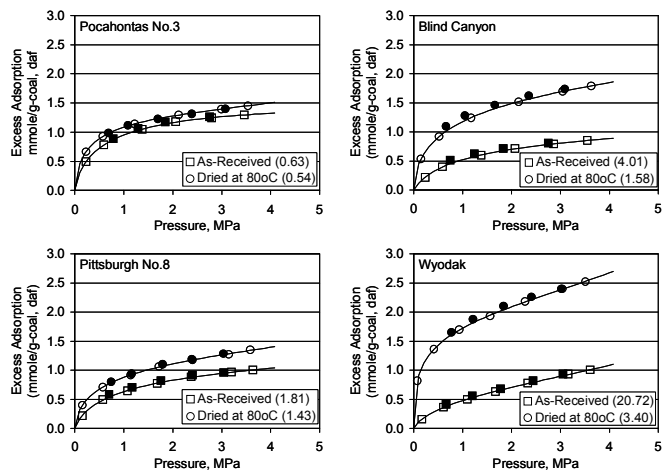


**Figure 1.** Excess adsorption of CO<sub>2</sub> on as-received and dried (at 80°C under vacuum for 20 hrs) Argonne coals. Open symbols: Adsorption, closed symbols: Desorption

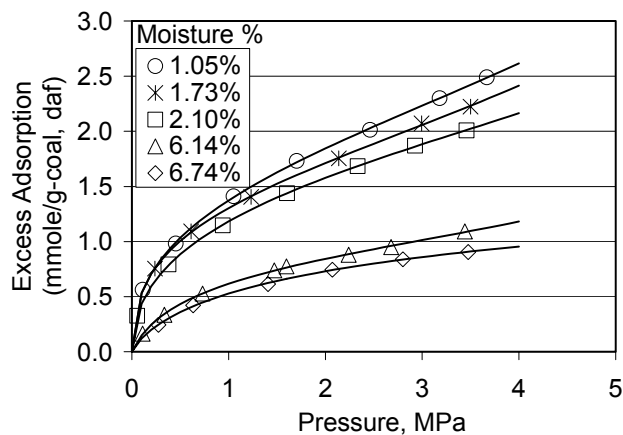


**Figure 2.** Adsorption isotherms of CO<sub>2</sub> on Argonne Premium Illinois No.6 coals having different moisture content

### Discussion

The adsorption capacities of the wet coals are lower than the dried coals and display an isotherm that becomes almost linear for low-rank coals. Using the modified adsorption equation (Eq.1) to interpret this data leads to the conclusion that the nearly linear portion of the isotherm results from a volumetric change that may be related to the swelling properties of the coals. The surface (or pore-filling) adsorption is reflected in the curved, Langmuir-like portion of the isotherm which is more pronounced for higher rank coals and lower pressures.

If the CO<sub>2</sub> adsorption capacities are calculated by substituting an appropriate adsorption expression for the  $n^{ads}$  into Eq.1, e.g. as  $n^{ex}$  in Eq.2, the dependence of the adsorption on the moisture content appears to be linear as seen in Figure 3. The slopes of the lines are indicative of the importance of water to the adsorption of CO<sub>2</sub>. Conversion of g water per 100 g coal (% moisture) to millimoles of water lost gives a slope of 1.1 moles of water lost per mole of CO<sub>2</sub> adsorbed for the higher rank coals. Thus, for the higher rank coals, it appears that the effect of moisture on the adsorption may be simply one of competition of H<sub>2</sub>O and CO<sub>2</sub> for the same binding sites.

However, the slopes become progressively smaller as one moves through the mid-rank to the low-rank coals. The slopes of the Wyodak and Beulah Zap coals are closer to 8 moles of water lost per mole of CO<sub>2</sub> adsorbed. Thus, in the case of low-rank coals, either many adsorption sites that are active for H<sub>2</sub>O adsorption are unfavorable for CO<sub>2</sub> adsorption, perhaps because they are too polar, or, possibly, clusters of water molecules block each CO<sub>2</sub> binding site.

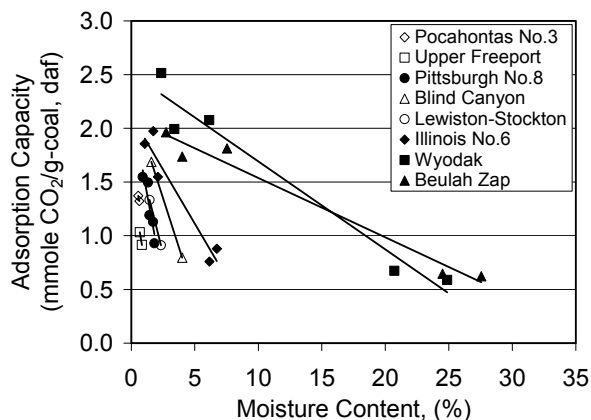


**Figure 3.** Adsorption of CO<sub>2</sub> on Argonne Premium coals as a function of moisture content.

### Conclusions

The presence of moisture significantly decreases the CO<sub>2</sub> adsorption capacities of coals, regardless of rank. Therefore, CO<sub>2</sub> adsorption isotherms of dried coals may not provide the information needed to interpret or model CO<sub>2</sub>.

### References

- Shroeder, K., Ozdemir, E., and Morsi, B.I., *First National Conference on Carbon Sequestration*, 2001, May 14-17, 2001, Washington D.C.
- Joubert, J., I., Grein, C., T., and Bienstock, D., *Fuel*, **1973**, 52, 181-185
- Joubert, J., I., Grein, C., T., and Bienstock, D., *Fuel*, **1974**, 53, 186-191
- Gregg, S., J., and Sing, K., S., W., *Adsorption, Surface Area and Porosity*, Academic Press, New York, 1982
- Martinez, J.M.M., Marcia, R.T., and Hazeleger, M.C.M., *Fuel*, **1995**, 74, 111-114
- Levy, J., H., Day, S., J., and Kilingley, J., S., *Fuel*, **1997**, 76, 813-819
- Suuberg, E.M., Otake, Y., Yun, Y., and Deevi, S.C., *Energy & Fuels*, **1993**, 7, 384-392
- Vorres, K., S., *Users Handbook for the Argonne Premium Coal Sample Program, (ANL/PCSP-93/1)*, Argonne National Laboratory, Argonne, Illinois 1993
- Ozdemir, E., Schroeder, K., and Morsi, B.I., *Am. Chem. Soc., Div. Fuel Chem. Prepr.*, **47** (1), 12-13, **2002**

## CO<sub>2</sub> Sequestration with Oriskany Brine

Y. Soong, J. R. Jones, D. K. Harrison, A. L. Goodman, J. P. Baltrus,  
S. W. Hedges and G. F. Walbert<sup>1</sup>

U.S. Department of Energy, National Energy Technology  
Laboratory,

P.O. Box 10940, Pittsburgh, PA 15236

<sup>1</sup>Parsons Project Services, Inc. P.O. Box 618, South Park, PA 15129

### Introduction

CO<sub>2</sub> is the major gas contributor to global warming [1]. Many techniques to capture and store CO<sub>2</sub> are currently being investigated. CO<sub>2</sub> injection into saline aquifer formations is one of the promising geologic CO<sub>2</sub> sequestration options. It is attractive, because there are regionally extensive aquifers capable of accepting large volumes of CO<sub>2</sub> (500 Gt. of CO<sub>2</sub>) from power plants without the need for long transport pipelines. Upon injection of CO<sub>2</sub> into saline aquifers, CO<sub>2</sub> may be stored by hydrodynamic and/or mineral trapping. The most critical concern of hydrodynamic trapping is the potential for CO<sub>2</sub> leakage through imperfect confinement. In mineral trapping, CO<sub>2</sub> is converted into carbonate minerals by a series of reactions with aqueous ions found in the saline aquifer. Various carbonates such as calcite, magnesite, dolomite, and siderite can be formed in the brine aquifer by mineral trapping [1,2]. However, conversion of CO<sub>2</sub> to stable carbonate minerals is expected to be slow. Researchers from the Alberta Research Council in Canada [2] calculated times for precipitation of the various carbonates to occur on the order of hundreds of years. These results suggest that mineral trapping may contribute significantly to CO<sub>2</sub> sequestration within saline aquifers but only in the long term.

Sass et al., [3] studied CO<sub>2</sub> and brine reactions with mineral rocks for 7 days at a pressure of 5.44 MPa and 110 °C. They found increased levels of Ca, Mg, and carbonate in solution, which were due to the dissolution of dolomite. Lebro'n and Suarez [4] reported the precipitation rate of calcite increased as the partial pressure of CO<sub>2</sub> increased (0.035 to 10 kPa). However, no extensive laboratory studies directed at the sequestration of CO<sub>2</sub> in brine aquifers have been conducted. As such, brine from the Oriskany Sandstone aquifer of the Appalachian Basin is examined to assess its ability to sequester CO<sub>2</sub> in the near term via the mineral trapping pathway upon reaction with CO<sub>2</sub>. This study attempts to evaluate the ability of such brines alone to serve as a mineral trapping medium. It is prudent to investigate the variables that effect mineral carbonates formation in brines in the absence of complication factors introduced by the presence of formation rocks. Specifically the effects of pH, CO<sub>2</sub> pressure, and temperature on the reaction between CO<sub>2</sub> and brine samples to form carbonate minerals were investigated. The optimum reaction conditions that favor the formation of mineral carbonates were investigated with autoclave experiments and geochemical modeling.

### Experimental

To examine the mineral trapping under controlled temperature and pressure conditions in an autoclave reactor, brine samples were collected from the Oriskany Sandstone in Indiana County, PA., at a depth of 2,550 m. No effort was made to prevent oxygen from contacting the brine. The brine was tested as received without further filtration. Brine carbonation experiments were carried out in a ½ liter autoclave. The details of the experimental setup are shown elsewhere [5]. The brine was used either as received, or the pH was adjusted before reaction by adding KOH. The effects of pH (3.6 to 11), reaction time (1 to 6 hours), CO<sub>2</sub> pressure (0.34 to 7.63 MPa), and temperature (50 to 170°C) on brine carbonation were

investigated. The brine carbonation reactions were also modeled with the computer program PHREEQC version 2. The simulation results were used as a guide in determining specific experimental conditions to investigate with the autoclave reactor.

### Results and Discussion

The mineral dolomite was not allowed to precipitate in the simulation even though the saturation index for it was positive. The kinetics for dolomite precipitation is relatively slow and it is likely that this mineral may not precipitate out of solution [6]. In addition, XRD analysis of the solid precipitate from the autoclave reactions did not detect dolomite.

The autoclave experiments and simulations were conducted to study the reaction of CO<sub>2</sub> with brine samples as a function of pH at constant temperature (155°C) and CO<sub>2</sub> pressure (6.87 MPa) (Fig. 1). After reaction, the pH of the solution was measured and found to be lower than the starting pH (Fig. 1a – solid circles). A similar trend between the pH before reaction and the pH after reaction with CO<sub>2</sub> is observed in the simulation results (Fig. 1a – dashed line). The pH of the brine decreases following reaction with CO<sub>2</sub> because CO<sub>2</sub> dissolves in solution to form carbonic acid, H<sub>2</sub>CO<sub>3</sub>, thus decreasing the pH. In addition, CO<sub>2</sub> not present after reaction due to the reactor was depressurized. As Ca and other metals are removed from solution by precipitation, the remaining solution become more acidic.

As the initial pH of the raw aqueous brine was increased from 3.6 to 11 by adding KOH, the concentration of the aqueous ion Ca in the reacted brine decreased by 25 %. The total grams of precipitate increased from 0.08 to 7.5 g/L (Fig. 1b – solid circles). The simulation results indicate a similar trend as pH increases, the total grams of solid precipitate increases from 0.1 grams at pH 2.7 to 30.5 grams at pH 11 (Fig. 1b – dashed line). However, the total grams of precipitate predicted by the model deviates significantly from experimental observations in that the model predicts almost four times as much solid precipitate than what is observed experimentally. This may be due to the fact the simulation is predicting total grams of precipitate under equilibrium conditions, while the total grams of solid precipitate from the autoclave experiments is measured after six hours of reaction followed by degassing CO<sub>2</sub> and cooling down to 25 °C. Although the experimental and model results differ on the amount of solid precipitate formed as pH is increased, both results follow the same general trend in that the total mass of solid precipitate increases as the pH increases (Fig. 1b). Only 0.09 g of Ca per gram of precipitate was observed at the initial brine pH of 7.2. Significantly more Ca precipitate was observed after the initial brine pH was increased to 9 and higher. The concentration of solid Ca precipitate increased by one order of magnitude (Fig. 1c). Both XRD analyses of the solid precipitate from the autoclave reactions and simulation results identified CaCO<sub>3</sub> and Fe<sub>2</sub>O<sub>3</sub> to be the main components of the solid samples at pH values greater than 9. Thus, as the pH is increased from 9 to 11, the grams of CaCO<sub>3</sub> per total grams of precipitate (g Ca/g ppt) (Fig. 1c).

Next, a series of autoclave experiments and simulations were conducted to study the reaction of CO<sub>2</sub> with brine samples as a function of pressure at constant pH (pH = 11.0) and temperature (155 °C). The CO<sub>2</sub> pressure was varied from 0.34 to 7.64 MPa. The pH after reaction, concentration of the aqueous components, total grams of precipitate, and grams of Ca per total grams of precipitate versus pressure did not change significantly as pressure was increased. From these results, pressure does not seem to play a large role in the formation of carbonate minerals as long as a minimum CO<sub>2</sub> pressure is maintained in the reactor. Therefore, high CO<sub>2</sub> pressures are not required for the precipitation of carbonate minerals.

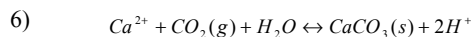
Finally, a series of autoclave experiments and simulations were conducted to study the reaction of CO<sub>2</sub> with brine samples as a

function of temperature at constant pH (pH = 11.0) and CO<sub>2</sub> (0.34 MPa) pressure (Fig. 2a-c). The temperature was varied from 50 to 170 °C. The pH after reaction, concentration of the aqueous components, total grams of precipitate, and grams of Ca per total grams of precipitate versus temperature changed very little for the autoclave experiments (Fig.2a-c). However, the simulation results predict a general increase in total grams of precipitate and grams of Ca per total grams of precipitate versus temperature. This may be due to the fact the simulation is predicting total grams of precipitate under equilibrium conditions, while the total grams of solid precipitate from the autoclave experiments is measured after six hours of reaction followed by degassing CO<sub>2</sub> and cooling down from reaction temperature to ambient condition. From these results, the experimental data suggest that temperatures above 50°C do not play a large role in the formation of carbonate minerals.

Mineral trapping occurs via reactions (1-5) shown below. CO<sub>2</sub> gas dissolves into solution (1). Carbonic acid is formed (2), which then dissociates into bicarbonate (3) and carbonate ions (4). Thus, pH of an aqueous solution decreases with the addition of CO<sub>2</sub> [4,7]. Then ions such as Ca, Mg, and Fe react with the carbonate ions to form minerals such as calcite, dolomite, siderite, and magnesite (5a-5d), respectively. 1) CO<sub>2</sub> (gas) → CO<sub>2</sub> (aq); 2) CO<sub>2</sub> (aq) + H<sub>2</sub>O → H<sub>2</sub>CO<sub>3</sub>; 3) H<sub>2</sub>CO<sub>3</sub> → H<sup>+</sup> + HCO<sub>3</sub><sup>-</sup>; 4) HCO<sub>3</sub><sup>-</sup> → H<sup>+</sup> + CO<sub>3</sub><sup>2-</sup>; 5a) Ca<sup>++</sup> + CO<sub>3</sub><sup>2-</sup> ↔ CaCO<sub>3</sub> (calcite); 5b) Ca<sup>++</sup> + Mg<sup>++</sup> + CO<sub>3</sub><sup>2-</sup> ↔ CaMg(CO<sub>3</sub>)<sub>2</sub> (dolomite); 5c) Fe<sup>++</sup> + CO<sub>3</sub><sup>2-</sup> ↔ FeCO<sub>3</sub> (siderite); 5d) Mg<sup>++</sup> + CO<sub>3</sub><sup>2-</sup> ↔ MgCO<sub>3</sub> (magnesite)

The pH of the brine affects the reaction rate and species precipitated. In a closed system dissolved carbon dioxide, CO<sub>2</sub>(aq) and H<sub>2</sub>CO<sub>3</sub> (carbonic acid) predominate at low pH, HCO<sub>3</sub><sup>-</sup> (bicarbonate) dominates at mid pH, and CO<sub>3</sub><sup>2-</sup> (carbonate) rules at high pH. The solubility of carbonate also increases as the pH decreases. Thus, aqueous-phase equilibrium with CO<sub>2</sub>(g) promotes carbonate precipitation under basic conditions, while acidic conditions favor carbonate dissolution. Therefore, to favor the precipitation of mineral carbonates, the pH must be basic. As demonstrated here, brine pH affects whether carbonate minerals will precipitate from solution (Fig. 1c).

Mineral trapping is also controlled by CO<sub>2</sub> pressure and temperature but by a lesser extent when compared to pH. Temperature and pressure also play an important role in determining the solubility of CO<sub>2</sub> in solution [8]. However, experimental results suggest that temperature does not play a major role in brine carbonation above 50°C (Fig. 2). The CO<sub>2</sub> pressure affects the CO<sub>2</sub>-brine reaction, but it is very dependent upon pH. Dreybodt et al [9] conducted the study of the precipitation kinetics of calcite in the system CaCO<sub>3</sub>-H<sub>2</sub>O-CO<sub>2</sub>. They concluded that the rate limiting step is equation 3. If the same rate-limiting step applied to the CO<sub>2</sub>-brine system, then the pH of the system is dominated. Basic environments, pH=11, favors the formation of HCO<sub>3</sub><sup>-</sup> and CO<sub>3</sub><sup>2-</sup> and finally the formation of CaCO<sub>3</sub>. The formation of calcite would ease, once the basic conditions changed. Therefore, pH as more impact on the carbonation reaction than temperature and pressure. The overall equilibrium equation for calcite formation can be described by equations 6 and 7:



$$7) \quad K = \frac{[H^+]^2}{[Ca^{2+}]P_{CO_2}}$$

According to equation 7, the calcite formation is dependent upon the hydrogen ion concentration, CO<sub>2</sub> pressure, and Ca ion concentration. When the CO<sub>2</sub> pressure increases at the constant

initial pH, the amount of calcite precipitate remains the same. As the CO<sub>2</sub> pressure is increased, the pH decreases because carbonic acid is formed. As CO<sub>2</sub> pressure continues to increase, the pH drops from 11 to 4.5. At low pH values, calcite not longer precipitates from solution. As discussed earlier, calcite precipitation is favored at high pH, while calcite dissolution is favored at low pH. Thus the amount of Ca precipitate is limited by the pH not the CO<sub>2</sub> pressure as long as a minimum pressure is maintained. In order to increase the amount of CaCO<sub>3</sub> precipitation with increasing CO<sub>2</sub> pressure, the pH will need to be buffered at values higher than 9.0.

## Conclusions

The reactions between CO<sub>2</sub> and brine samples collected from the Oriskany Formation in Indiana County, PA were investigated experimentally using a ½ liter autoclave under various conditions and theoretically using the geochemical code PHREEQC. The results indicate that the amount of calcite precipitate depends primarily on the pH of the brine. The CO<sub>2</sub> pressure and temperature have lesser impact on the formation of carbonates.

## References

- DOE report, DOE/SC/FE-1, Carbon Sequestration Research and Development, December 1999.
- Hitchon, B. Gunter, W. D. Gentsis, T. and Bailey, R. T., *Ener. Conv. & Man.* 40 (1999) 825.
- Sass, B. N., Gupta, J. Ickes, J., Egelhard, M., Bergman, P.D. and Byaer, C; Conference CD, 1<sup>st</sup> National Conference on Carbon Sequestration, Washington, D.C., May 15-17, 2001.
- Lebro'n, I and Suarez, D. L., *Geochim. Cosmochim. Acta* 62 (1998) 405.
- Soong, Y., Jones, J. R., Hedges, S. W., Harrison, D. K., Knoer, J. P., Baltrus, J. P., and Thompson, R. L., *Am. Chem. Soc. Div. Fuel Chem.* 2002, 47 (1) 43
- Lasaga A. C. (1998) "Kinetic Theory in the Earth Science," Princeton University Press, 811.
- Krauskopf K. B., (1979) "Introduction to Geochemistry", McGraw-Hill, New York, 43.
- Enick, B. M. Klara, S. M., *Chem. Eng. Comm.* 90 (1990) 23.
- Dreybodt, W., Eisenlohr, L., Madry, B., and Ringer, S., (1997) *Geochim. Cosmo. Acta*, 61, 3987.

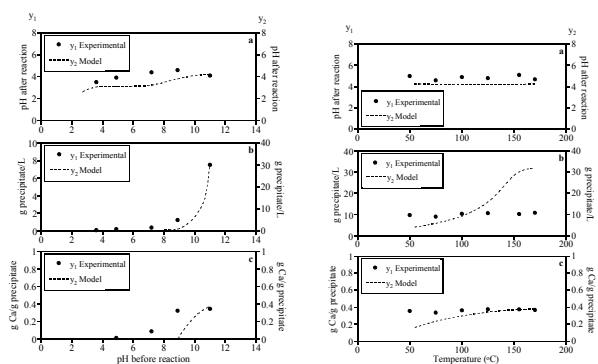


**Fig 1.** Brine carbonation as function of pH at 6.87 MPa CO<sub>2</sub> and 155 °C (left).

**Fig 2.** Brine carbonation as function of temperature at 0.343 MPa CO<sub>2</sub> and pH 11 (right).

# UTILIZATION OF STATIC MIXER ON THE INJECTION OF LIQUID CO<sub>2</sub> INTO WATER FOR THE OCEAN DISPOSAL

Hideo Tajima, Akihiro Yamasaki, and Fumio Kiyono

National Institute of Advanced Industrial Science and Technology  
16-1 Onogawa, Tsukuba, Ibaraki 305-8569, Japan

## Introduction

Several scenarios of CO<sub>2</sub> disposal into the ocean have been proposed for a long-term sequestration as a counteraction measure for global warming. In the disposal process of liquid CO<sub>2</sub>, especially, liquid CO<sub>2</sub> would be released from a pipeline through a nozzle to the ocean at the depth deeper than 500 m<sup>(1)</sup>. Since the density of liquid CO<sub>2</sub> is smaller than that of seawater at the depth shallower than 3000 m, the released CO<sub>2</sub> droplets would ascend to the ocean surface. During the droplet ascending process, the CO<sub>2</sub> would be dissolved into the seawater from the droplets, and the ascending speed would decrease by the reducing size of the droplets. The dissolution process should be completed before reaching the sea surface. Since the ascending and dissolution behavior depends on the size of the released CO<sub>2</sub> droplets, the releasing size of the droplet should carefully designed and controlled on the injection. On the other hand, the effect of CO<sub>2</sub> hydrate should be considered in the disposal process of liquid CO<sub>2</sub>, because the thermodynamic condition of CO<sub>2</sub> hydrate formation would normally be satisfied in the ocean at depths greater than 500 m ( $T < 283$  K and  $p > 44.5$  bar<sup>2)</sup>). The nozzle of the CO<sub>2</sub> pipeline could be blocked by the formation of solid CO<sub>2</sub> hydrate upon injection and sequent the agglomeration of the hydrates, and the blockage should be prevented for a continuous and stable injection process.

In this research, a novel injection process of liquid CO<sub>2</sub> into the ocean by utilization a static mixer was proposed as a possible solution for the above difficulties, and the hydrodynamic behavior of the liquid CO<sub>2</sub> in water was studied through laboratory-scale experiments for obtaining basic knowledge for the disposal process design.

## Outline of utilization of static mixer on CO<sub>2</sub> disposal process

Figure 1 shows a conceptual drawing for the outline of the new disposal of CO<sub>2</sub> in the ocean. Liquid CO<sub>2</sub> is sent to the depths about 500m in the ocean through a pipeline, then disposed of through a static mixer in which liquid CO<sub>2</sub> was mixed with the ambient seawater.

The structure of a typical static mixer is shown in Figure 2. In the static mixer, elements are arranged and fixed inside a straight tube. The element could make the incoming fluid to be turbulent. The flow in the static mixer is close to a piston flow, and uniform radial mixing could be realized. The energy consumption for the mixing is only pressure droplet consumed by flowing through the static mixer, which is much lower than the power consumption by the stirring process with a stirred-tank type mixer.

The advantages of utilizing a static mixer in the disposal process of liquid CO<sub>2</sub> in the ocean would be the following: (1) droplet size control, (2) blockage control, and (3) energy saving process. With a proper design of the static mixer, continuous formation and disposal process of CO<sub>2</sub> hydrate could be realized as an extended version of the present process. Since no literature data are found for the behavior of liquid CO<sub>2</sub> in the static mixer, the hydrodynamic behavior of liquid CO<sub>2</sub> and water in a static mixer was examined in a laboratory scale experimental apparatus in this study.

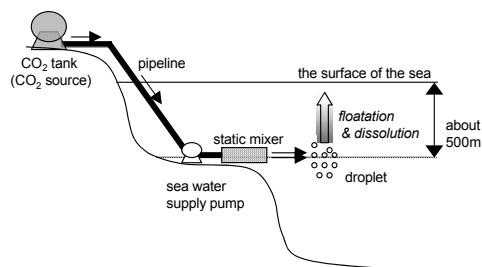


Figure 1. Concept drawing for utilization of static mixer on CO<sub>2</sub> injection into the ocean

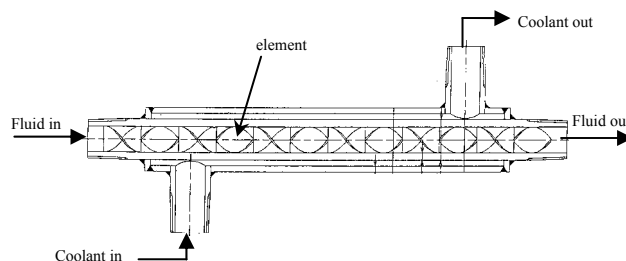


Figure 2. Noritake static mixer (Type: 3/8-N10-522-N)

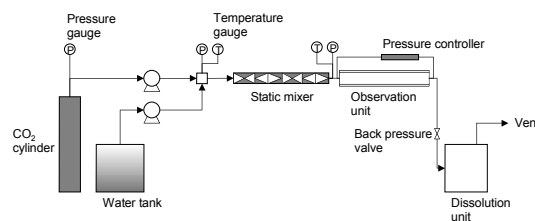


Figure 3. Schematic drawing of the apparatus of hydrate

## Experimental

The schematic flow diagram for the experimental apparatus is shown in Figure 3. Liquid CO<sub>2</sub> with the highest purity (> 99.90%) and deionized water were introduced to the static mixer by a high-pressure pump (Nippon Seimitsu Co., Ltd., NP-AX-70, Fuji Pump Co., Ltd., 2JN224-10V) after pre-cooling to a desired temperature. The static mixer was specially designed and made for high-pressure and low temperature conditions by Noritake Co., Ltd., Japan based on the style: 3/8-N10-522-N. The behavior of the mixture was observed in a transparent observation unit made of polycarbonate tube (inner diameter 10.6 mm, length 300 mm) which was connected downstream side of the static mixer. The temperature of the system was controlled by the fluid flow in the jacket on the flow lines where temperature-controlled coolant of a mixture of water and ethylene glycol was circulated from a cooling unit. The behavior of the fluid mixing was recorded through the observation part with a high-speed video camera (Photron Ltd.; maximum 500 frame per second). Then, the video data was captured and analyzed by a Power Macintosh G4 computer using the public domain ImageJ (ver.1.27) program (developed at the U.S. National Institute of Health and available from the Internet, <http://rsb.info.nih.gov/nih-image/>).

## Results and Discussion

**Injection of CO<sub>2</sub> into Water Using Static Mixer.** Figure 4 shows the CO<sub>2</sub> droplet formed in the static mixer. The pressure was 7.0 MPa, Note A) is out of hydrate formation condition and B) is within it. For the higher temperature conditions without hydrate formation, the CO<sub>2</sub> droplets could be formed in the static mixer, but would be merged to form a larger droplet. On the other hand, the merge of droplets would be prevented by the surface hydrate film for the lower temperature conditions; instead, sometimes grape-like agglomerates were formed through the contact of droplets.



A) 289K

B) 278K

**Figure 4.** Effect of hydrate formation on CO<sub>2</sub> droplet

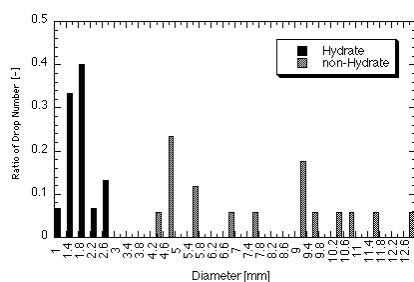


**Figure 5.** Distribution of CO<sub>2</sub> droplet diameter

Figure 5 shows the measured size distribution of CO<sub>2</sub> droplets. The droplet size for the lower temperature condition, the distribution of the diameter was limited in a narrow range of 1 to 2.6 mm. Thus, CO<sub>2</sub> droplets with relatively uniform size could be obtained for the condition with hydrate formation. This would express significantly the uniform distribution in an essential property of a static mixer.

### Effect of water and CO<sub>2</sub> flow rate on droplet diameter.

Figure 6 shows the effect of the water flow rate on the liquid CO<sub>2</sub> droplets formation in the static mixer with a constant CO<sub>2</sub> flow rate. The temperature was 276 K, and the pressure was 7.0 MPa for all the cases, which is in the hydrate formation region. The flow rate was denoted by the Reynolds number based on the diameter of the static mixer, and the viscosity and flow rate of pure water. For all the cases, the hydrate formation on the surface was noticed. With an increase in the flow rate, the average diameter decreased and the distribution became narrower. The average diameter decreased rapidly under lower Reynolds number conditions of laminar flow region. At higher flow conditions, the average diameter change was less sensitive to the flow conditions. Note the agglomeration of the droplets was scarcely observed for the higher Reynolds number (> 3000). The above results indicate that the mixing by the static mixer becomes more vigorously and more uniformly under higher flow conditions.

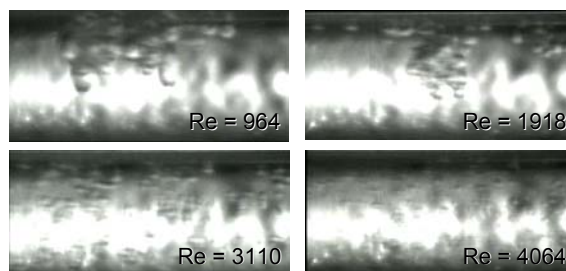


**Figure 6.** Effect of Reynolds number on droplet diameter

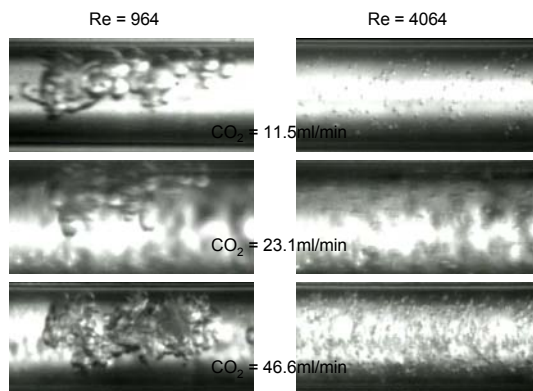


**Figure 7.** Effect of CO<sub>2</sub> flow rate on droplet diameter

Figure 7 shows the effect of CO<sub>2</sub> flow rate with a constant water flow rate and temperature (276 K), pressure (7.0 MPa). At the lower flow rate of water (Re=964), which is in the laminar flow region, larger droplets of liquid CO<sub>2</sub> were observed, and the droplet size decreased remarkably with an increase in the CO<sub>2</sub> flow rate. On the other hand, smaller droplets were observed at higher Reynolds number of 4064, and the size of the droplets seems independent of the CO<sub>2</sub> flow rate. The above results indicate that the droplet size of liquid CO<sub>2</sub> could be significantly affected by the flow condition of liquid CO<sub>2</sub> as well as that of water.

**Fate of the CO<sub>2</sub> disposal through the static mixer.** Assuming the releasing depth of liquid CO<sub>2</sub> 500 m, the calculation showed the initial diameter should be smaller than 9.1 mm to be dissolved completely before reaching the sea surface. To avoid the vaporization, the initial diameter of the droplet should be smaller than 4.0 mm. When injected through the static mixer, the droplet size is under the above critical value for the conditions studied in this research. As the droplets with the average diameter 0.4 mm are formed through the static mixer, the energy consumption per 1g of CO<sub>2</sub> is estimated to be about 0.35 MJ/t-CO<sub>2</sub>. This value is negligible when compared with the energy consumption for the separation or liquefaction energy from the flue gas (48.0 J/g-CO<sub>2</sub> for separation, 336.2 J/t-CO<sub>2</sub> for liquefaction<sup>1)</sup>). Thus, utilization of static mixer would be very suitable for the liquid CO<sub>2</sub> injection disposal in the ocean.

## References

- (1) Halmann, M. M.; Steinberg, M. In *Greenhouse Gas Carbon Dioxide Mitigation: Science and Technology*; Lewis Publishers: Boca Raton, 1999
- (2) Sloan E. D., In *Clathrate Hydrates of Natural Gases*, 2 Ed, Dekker: New York, 1998

# FORMATION AND GROWTH OF CO<sub>2</sub> HYDRATE PARTICLES IN A FLUIDIZED BED REACTOR

Akihiro Yamasaki\*, Satoko Takano, Minoru Fujii, Yukio Yanagisawa, Hideo Tajima, Fumio Kiyono

School of Frontier Sciences, The University of Tokyo  
7-3-1 Hongo, Bunkyo-ku, Tokyo, JAPAN

\*Institute for Environmental Management Technology  
National Institute of Advance Industrial Science and Technology  
16-1 Onogawa, Tsukuba, JAPAN

## Introduction

Several carbon sequestration scenarios have been proposed as counteraction measures to the global warming issue including ocean sequestration and underground sequestration. In the sequestration scenarios, CO<sub>2</sub> captured and separated from the flue gas of the concentrated emission sources of anthropogenic CO<sub>2</sub> such as thermal power plants and steel industries is targeted. The ocean sequestration scenarios may have advantages over other scenarios from the viewpoints of the capacity and the sequestration term. The forms of CO<sub>2</sub> upon discharge for the ocean sequestration scenarios could be gaseous, liquid, and clathrate hydrate. Albeit the difference in the form of CO<sub>2</sub> upon disposal in the oceans, the discharged CO<sub>2</sub> will eventually be dissolved into the ambient seawater, and sequestered there for a certain period before releasing to the atmosphere. The dissolution of CO<sub>2</sub> would cause a pH change of the ambient seawater and consequently cause an impact to the marine ecosystem. In order to obtain the public acceptance for the sequestration practice, such environmental impact should be controlled and minimized. From the viewpoint of the environmental impact, the disposal scenario of CO<sub>2</sub> hydrate would be most appropriate because of the following reasons.

1. Since the density of CO<sub>2</sub> hydrate is greater than the seawater at any depth of the ocean, the disposed hydrate particles should descend toward the ocean bottom. This is in contrast with the cases of disposal of liquid or gaseous CO<sub>2</sub>: liquid CO<sub>2</sub> is less dense than the seawater unless the depth is greater than 3000 m, and gaseous CO<sub>2</sub> is much less dense, the disposed CO<sub>2</sub> in such fluid phases will ascend to the sea surface. Thus, to avoid the risk of reemission of CO<sub>2</sub> to the atmosphere, the dissolution should be completed before reaching the surface.
2. The CO<sub>2</sub> hydrate particles would release CO<sub>2</sub> into the seawater due to its instability caused by the difference in the chemical potential of CO<sub>2</sub> between in the seawater and the hydrate. However, the releasing rate is known to be much smaller for CO<sub>2</sub> hydrate than that for liquid CO<sub>2</sub> from laboratory experiments simulating the deep ocean conditions.

The above-mentioned natures of CO<sub>2</sub> hydrate would lead us that the environmental impact caused by the released CO<sub>2</sub> could be more controllable for the CO<sub>2</sub> hydrate disposal by choosing a proper initial diameter and the disposal depth of the hydrate particles.

Disadvantage of the hydrate disposal process might be its energy consumption in the hydrate formation process because it requires high pressure (> 4.5 MPa) and low temperature (< 283 K) conditions. This difficulty by the thermodynamic constraint could be resolved by the submerged reactor at the depth greater than 450 m. However, to form hydrate particles with proper density, substantial energy consumption might be necessary to realize the highly turbulent condition to enhance the interfacial mass transfer in a stirred tank type reactor, which is commonly used for the hydrate

formation process in a laboratory scale. Moreover, it is difficult to control the particle size of the hydrate in such a reactor.

Although intensive studies have been conducted for the formation process of CO<sub>2</sub> hydrate, no contribution could be found in the literature from the viewpoint of effective formation process of CO<sub>2</sub> hydrate particles with controlling the size. The authors have proposed here a concept of a novel process of CO<sub>2</sub> hydrate formation in a fluidized-bed type reactor. In this paper, the concept of the proposed process has been examined by a laboratory scale experiments.

## Concept of hydrate formation process in a fluidized bed type reactor

The conceptual drawing for the proposed process of hydrate formation was shown in Fig. 1. The reactor is a three-phase fluidized bed type reactor where a mixture of CO<sub>2</sub> hydrate particles (solid), liquid CO<sub>2</sub> (liquid 1) and water (liquid 2) are in a circulated fluidization. Initially seed crystals of CO<sub>2</sub> hydrate would be supplied to the reactor with water saturated with CO<sub>2</sub> and liquid CO<sub>2</sub>. The hydrate formation would be induced by the flow at the interface of CO<sub>2</sub> hydrate particles and water. Due to the difference in the solubility of CO<sub>2</sub> in water and the molar fraction of CO<sub>2</sub> in the hydrate crystals, the hydrate formation would result in a decrease in the concentration of CO<sub>2</sub> in water, which could be compensated from the accompanied liquid CO<sub>2</sub> phase. The hydrate particles of which the diameter is larger than the fluidization region would cease the fluidization, and be taken out from the reactor. On the other hand, the small particles that are too small to be fluidized would be released off from the top of the reactor, and could be circulated to become seed crystals after separation. The fluidization conditions would be so designed that hydrate particles with a proper size for the disposal process could be obtained at the bottom of the reactor. The main target in this study is to investigate the growth process and hydrodynamic behavior of CO<sub>2</sub> hydrate particles in the fluidized bed reactor under various flow conditions.

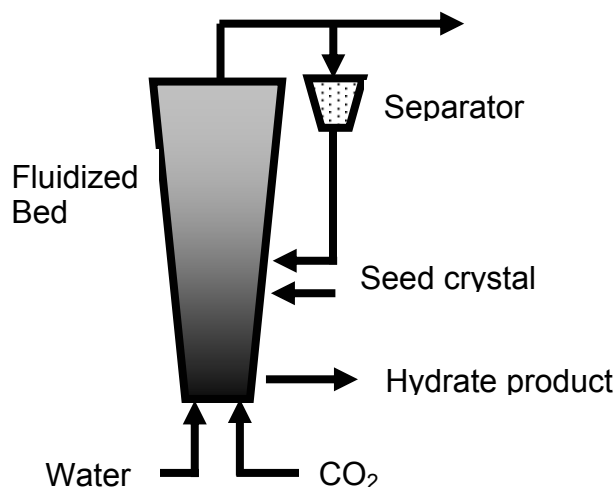


Fig. 1 Conceptual drawing for hydrate formation process in a fluidized bed type reactor

## Experimental

Figure 2 shows a schematic drawing for the experimental apparatus. The main fluidization part of the apparatus is a cylindrical

tube of polycarbonate of which the inner diameter is 47 mm, and the length is 470 mm. The tube is connected with the stirred tank type reactor with a ball-valve, which could be utilized for the seed crystal formation. The inner diameter of the stirred tank type reactor is 43 mm and the length is 150 mm. The stirring could be conducted by 3-propeller stirrer at the rate of 0 ~ 760 rpm. The circulation of the fluid could be carried out by a high-pressure pump of which the maximum flow rate is 10 L/min, which corresponds to the liner fluid velocity to be about 10 cm/s in the fluidization part. The temperature of the experimental system was controlled by the circulation of water/ethylene glycol mixture in the jacket. The temperature of the coolant was controlled by the cooling unit and the system temperature could be controlled within 0.5 °C of the fluctuations. The pressure of the system was controlled via cylinder-type pressure controller within  $\pm 0.2$  bar driven by nitrogen.

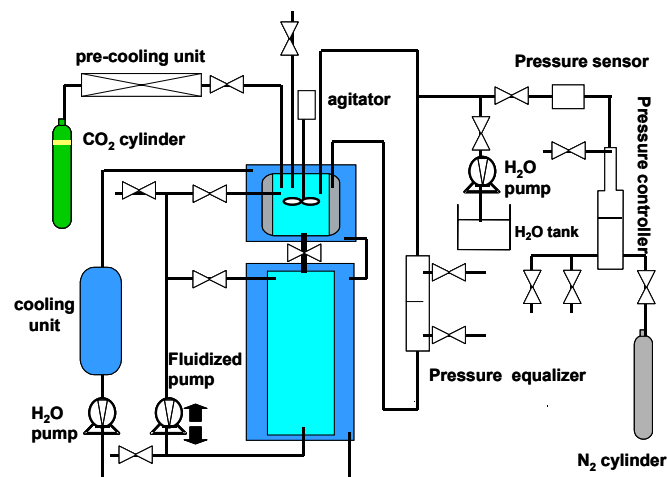


Fig.2 Schematic drawing for the experimental apparatus

## Results and Discussions

### Experimental procedure and preliminary results of hydrate formation

All the system (both the stirring vessel and the fluidization part) was first filled with deionized water under the atmospheric pressure and room temperature. Then a given amount of water was removed from the system to make room for the CO<sub>2</sub> insert. Liquid CO<sub>2</sub> was introduced to fill the system from the cylinder under stirring and flow condition. The system was cooled down gradually to the temperature for hydrate formation. At the same time, liquid CO<sub>2</sub> was added gradually to the system to compensate the increase in the solubility of CO<sub>2</sub> with decreasing temperature. Finally, the system was filled with water saturated with CO<sub>2</sub>. Since the CO<sub>2</sub> solubility is much smaller than the molar fraction of CO<sub>2</sub> in CO<sub>2</sub> hydrate, all the CO<sub>2</sub> supplied should be dissolved in water at the beginning. Then, supply of excess liquid CO<sub>2</sub> was started to realize a super saturation state. Under such conditions, the excess amount of CO<sub>2</sub> should eventually be converted to CO<sub>2</sub> hydrate via fluidization process. The conversion rate should depend on the hydrodynamic conditions in the system, *i.e.*, flow rate.

Due to the non-uniform temperature and concentration profiles in the system, crystals of CO<sub>2</sub> hydrate emerged even under the conditions below the solubility of CO<sub>2</sub> as shown in Figure 3 (a). The CO<sub>2</sub> hydrate crystal so formed had negative buoyancy in the water. This is in contrast to the CO<sub>2</sub> hydrate crystals formed by the agitation

of 2-phase fluid of liquid CO<sub>2</sub> and water, which had negative buoyancy at the initial stage of agitation (Fig.3 (b)). The difference in the apparent density would be due to liquid CO<sub>2</sub> drops might be remained in the hydrate particles for the case of agitation process. These hydrate particles were used as seed crystals for the further formation and growth of the CO<sub>2</sub> hydrate under the fluidization conditions.

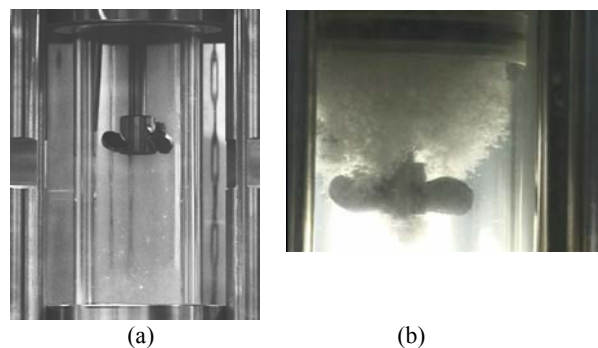


Fig.3 Hydrate crystals formed (a) without stirring, (b) with stirring

### Effect of the flow rate

The CO<sub>2</sub> hydrate particles were fluidized in water as shown in Figure 4 (time course, from left to right, about 10 s). The water flow rate was 5 L/min from the bottom to top, and the temperature was 275 K, the pressure was 6.4 MPa. During the fluidization, the increase of the average particle size was observed with time. The average size of the hydrate particles seemed smaller under higher flow rate conditions.

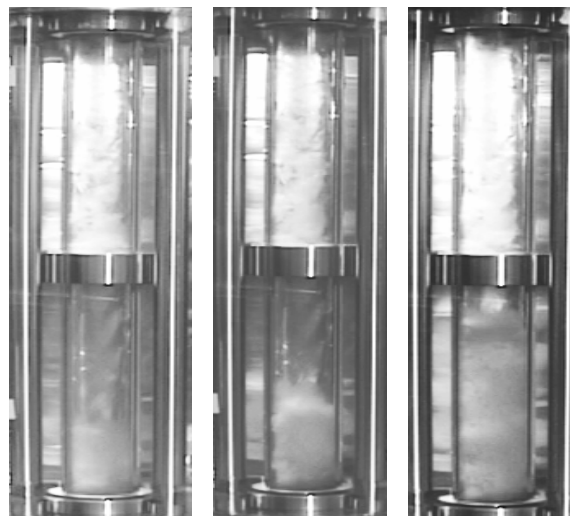


Figure 4 Fluidization of hydrate particles

## Conclusions

A new process of CO<sub>2</sub> hydrate formation was proposed by using a fluidized bed reactor was proposed. The laboratory experimental study indicated that CO<sub>2</sub> hydrate particles could be formed and grow in fluidized bed under proper flow conditions.

**Acknowledgement** This work is financially supported by RITE (Research Institute of Innovative Technology for the Earth Research) and The Japan Gas Association.

# PROPERTIES OF CARBON DIOXIDE HYDRATES CONCERNING THE SEQUESTRATION OF GLOBAL WARMING GASES

Fumio Kiyono, Hideo Tajima and Akihiro Yamasaki

Institute for Environmental Management Technology  
National Institute of Advanced Industrial Science and Technology  
16-1, Onogawa, Tsukuba, Ibaraki, 305-8569 Japan

## Introduction

Hydrates may play an important role in future carbon dioxide sequestration systems because hydrates can be used for both purpose of separation and sequestration. Sequestration of carbon dioxide in the hydrates form has many merits like long term storage and less environmental impact. In addition to that, if the hydrates technology were adopted in the separation process of carbon dioxide from flue gases, the total cost for the separation and the sequestration could be dramatically decreased.

According to the purpose, whether the separation or the sequestration, a coexisting phase with a hydrate phase is different. In case of the separation, the hydrate phase mainly coexists with a gas phase, but in the sequestration the hydrates phase is accompanied by a liquid phase. Thus, to build the total system which can separate carbon dioxide from flue gases by forming the carbon dioxide hydrates and then send them to the deep sea floor it is necessary to clarify behaviors of the hydrate phase in the whole phase space, especially when the hydrate phase only coexists with the vapor phase or the liquid phase.

In this paper, properties of carbon dioxide hydrates when coexisting with the vapor phase or the liquid phase are studied.

## Relationship between density, occupancy and mole fraction

One of the most important properties of hydrates relating to the sequestration may be the density of carbon dioxide hydrates. It determines whether hydrates can go downwards or upwards from the releasing point. The density of hydrates alters in accordance with the occupancy of carbon dioxide molecules in hydrate cages.

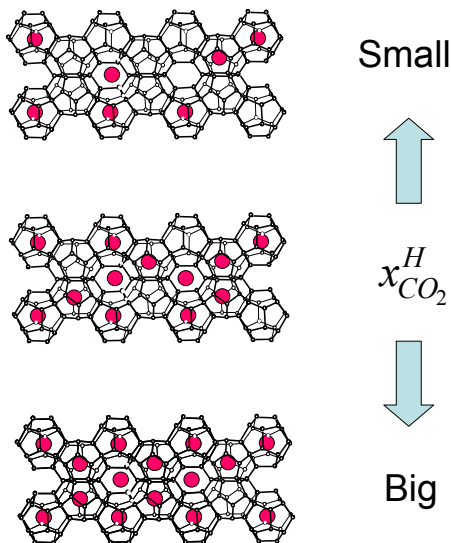


Figure 1. Mole fraction of guest component in hydrate phase

Figure 1 explains this relationship. The larger the occupancy is, the higher the density of hydrates and the mole fraction of carbon dioxide in the hydrates phase become. If we know the mass of a water molecule and a carbon dioxide molecule, we can calculate the density from the occupancy or the mole fraction.

## Behaviors of the hydrate phase on a phase diagram

To clarify the behaviors of a hydrates phase when coexisting with a vapor phase or a liquid phase the location of the hydrate phase on a phase diagram should be specified. Figure 2 illustrates possible arrangements of hydrates phases on the phase diagrams. In Fig.2 (a) the hydrates phase is represented by a line. If hydrates were the stoichiometric compound the hydrates phase would be designated by the line. In Fig.2 (b), (c) and (d) the hydrates phases are denoted by areas, but the inclination of each line which forms the boundary between other phases is different. In fig.2 (b) the hydrate line opposed to the liquid line, which express the equilibrium properties of hydrates coexisting with a liquid, has negative inclination, but the hydrate line opposed to the vapor line, which express the equilibrium properties of hydrates coexisting with a vapor, has positive inclination. In Fig.2 (c) the inclination of the both lines is positive and in Fig.2 (d) the inclination of the both lines is negative.

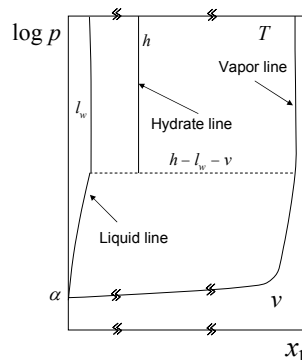


Figure 2. (a)

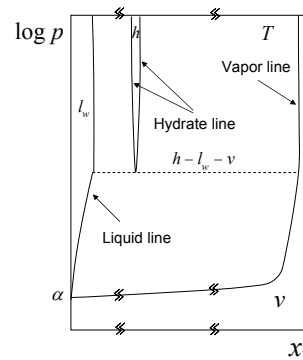


Figure 2. (b)

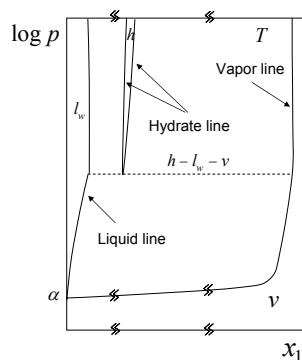


Figure 2. (c)

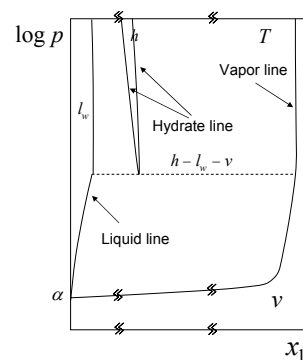


Figure 2. (d)

Figure 2. Possible arrangement of hydrates phases

### Qualitative analysis of hydrates' behaviors

Qualitative properties of the hydrates phase can be studied based upon the van der Waals and Platteeuw<sup>(1)</sup> equations. They derived these equations by applying a grand canonical distribution to guest molecules and a canonical distribution to water molecules. The equations consist of three equations.

$$\log f_w^H = \log f_w^\beta - \sum_{i=1}^2 v_i \log(1 + C_i f_i^H) \quad (1)$$

$$\theta_1 = \frac{C_1 f_1^H}{1 + C_1 f_1^H} \quad (2)$$

$$\theta_2 = \frac{C_2 f_2^H}{1 + C_2 f_2^H} \quad (3)$$

The equation (1) denotes the difference of fugacity of water in the hydrates phase and in the  $\beta$  lattice. The equation (2) represents the occupancy of CO<sub>2</sub> molecules in small cages, that is, the probability of finding a CO<sub>2</sub> molecule in a small cage, and equation (3) that in large cages. For our purpose equation (2) and (3) are useful.

It is obvious from the equation (2) and (3) that the value of the occupancy approaches to unity with the fugacity in the hydrates phase increasing. It means that the mole fraction of CO<sub>2</sub> in the hydrates phase becomes large and that the density of hydrates also becomes heavy.

If a hydrate phase coexists with a liquid phase, in equilibrium, the fugacity of CO<sub>2</sub> in the hydrate phase becomes equal to that in the liquid phase. Thus it is enough to clarify the dependence of the fugacity of CO<sub>2</sub> in the liquid phase on the pressure.

$$f_1^L = \phi_1^L x_1^L p \quad (4)$$

According to the equation (4) the fugacity of CO<sub>2</sub> increases with pressure, where the fugacity coefficient and the mole fraction of CO<sub>2</sub> in the liquid phase can be regarded to be constant comparing with the pressure change. So,

$$p \rightarrow \text{large} \quad f_1^H \rightarrow \text{large} \quad \theta_1, \theta_2 \rightarrow 1 \quad x_1^H \rightarrow \text{large}$$

When a hydrates phase coexists with a vapor phase, in equilibrium, the fugacity of CO<sub>2</sub> in the hydrate phase should be equal to that in the vapor phase. The derivative of the fugacity with respect to the pressure is expressed as follows.

$$\frac{\partial f_1^V}{\partial p} = \frac{f_1^V}{RT} v_1^V > 0 \quad (5)$$

Hence,

$$p \rightarrow \text{large} \quad x_1^H \rightarrow \text{large}$$

Summarizing the results of qualitative analysis, the inclination of hydrates lines should be both positive.

### Quantitative analysis of hydrates' behaviors

To clarify the behaviors of hydrate lines in the two-phase equilibrium such as liquid-hydrate or hydrate-vapor equilibrium under a constant temperature mass balance equations and diffusion stability equations were solved. Differing from the incipient calculation, to achieve this purpose, both equations have to be solved under constant temperature and pressure and mole fractions of water

and CO<sub>2</sub> in each phase must be sought simultaneously. Soave-Redlich-Kwong equation was employed for the equation of state, MHV2 for the mixing rule, and van der Waals-Platteeuw equation for the fugacity of water in the hydrates phase. Implicit expression of the fugacity of each gas component in the hydrates phase as a function of mole fractions had been given by Michelsen. Equations necessary for the calculation are as follows.

$$x_w^L + x_1^L = 1$$

$$x_w^H + x_1^H = 1$$

$$f_w^L = f_w^H$$

$$f_1^L = f_1^H$$

**Table 1. Behaviors of a liquid line and a hydrate line**

| Temperature | Pressure [Mpa] | Mole fraction in liquid phase | Mole fraction in hydrate phase |
|-------------|----------------|-------------------------------|--------------------------------|
| 277.6       | 2.11           | 0.0145                        | 0.1421                         |
| 277.6       | 4.11           | 0.0144                        | 0.1423                         |
| 277.6       | 6.11           | 0.0143                        | 0.1424                         |
| 277.6       | 8.11           | 0.0141                        | 0.1425                         |
| 277.6       | 10.11          | 0.0140                        | 0.1426                         |
| 277.6       | 12.11          | 0.0139                        | 0.1427                         |
| 277.6       | 14.11          | 0.0137                        | 0.1428                         |
| 277.6       | 16.11          | 0.0136                        | 0.1430                         |
| 277.6       | 18.11          | 0.0135                        | 0.1431                         |

**Table 2. Behaviors of a vapor line and a hydrate line**

| Temperature | Pressure [Mpa] | Mole fraction in vapor phase | Mole fraction in hydrate phase |
|-------------|----------------|------------------------------|--------------------------------|
| 277.6       | 2.11           | 0.99949                      | 0.1424                         |
| 277.6       | 2.61           | 0.99957                      | 0.1433                         |
| 277.6       | 3.11           | 0.99962                      | 0.1438                         |
| 277.6       | 3.61           | 0.99965                      | 0.1443                         |
| 277.6       | 4.11           | 0.99966                      | 0.1446                         |
| 277.6       | 4.61           | 0.99966                      | 0.1448                         |

Behaviors of the liquid line, the hydrates lines and the vapor line at the temperature of 277.6°K are listed in **Table 1** and **Table 2**. In case of the liquid-hydrate equilibrium, the mole fraction of CO<sub>2</sub> in the hydrate phase altered from 0.1421 to 0.1431 as pressure increased from 2.11MPa to 18.11MPa. In case of the vapor-hydrate equilibrium, the mole fraction of CO<sub>2</sub> in the hydrate phase varied from 0.1424 to 0.1448 with increasing the pressure from 2.11MPa to 4.61MPa.

The results of the quantitative analysis also show that the inclination of hydrates lines is both positive. Other thermodynamic properties like the latent heat, the heat capacity, etc can easily calculated from the phase equilibrium data.

### References

- (1) van der Waals; Platteeuw, J.C. *Adv. Chem. Phys.*, **1959**, 2, 1.

# Separation of CO<sub>2</sub> from Power Plant Flue Gas Using a Novel CO<sub>2</sub> “Molecular Basket” Adsorbent

Xiaochun Xu, Chunshan Song\*, Ronald Wincek, John M. Andresen, Bruce G. Miller, and Alan W. Scaroni

Clean Fuels and Catalysis Program, The Energy Institute, and Department of Energy & Geo-Environmental Engineering, The Pennsylvania State University, 209 Academic Projects Building, University Park, PA 16802, USA

\* Corresponding author. E-mail: csong@psu.edu; Tel: 814-863-4466; Fax: 814-865-3248

## Introduction

A considerable increase in the global atmospheric CO<sub>2</sub> concentration has raised concern about climate change and has led to a worldwide effort in research and development on control of CO<sub>2</sub> emissions.<sup>1,2</sup> The main CO<sub>2</sub> emission sources include fossil fuel-based electric power plants, vehicles, manufacturing plants for cement, limestone, hydrogen, ammonia, and commercial and residential buildings.<sup>2</sup> Capture and separation of CO<sub>2</sub> from stationary sources is considered as the first step for the control of CO<sub>2</sub> emission and its cost constitutes about three-fourths of the total cost of the control of CO<sub>2</sub> emission, e.g., carbon sequestration.<sup>3</sup> It is therefore important to explore new approaches for CO<sub>2</sub> separation.

Recently, a novel CO<sub>2</sub> “molecular basket” adsorbent, which showed a high CO<sub>2</sub> adsorption capacity and a high CO<sub>2</sub> selectivity, was developed in our laboratory.<sup>4-6</sup> The adsorbent was successfully applied in the separation of CO<sub>2</sub> from simulated flue gas.<sup>6</sup> In this paper, the separation of CO<sub>2</sub> from flue gas of a gas-/coal-fired power plant is reported.

## Experimental

The “molecular basket” adsorbent of MCM-41-PEI-50 (mesoporous molecular sieve of MCM-41 type with the polyethyleneimine PEI loading of 50 wt%) was used in the adsorption separation. The details on the preparation and characterization of this adsorbent are reported elsewhere.<sup>4,6</sup>

The adsorption separation of CO<sub>2</sub> from power plant flue gases was investigated. Both the gas-fired and the coal-fired flue gases were used as feed gases. The composition of the gas-fired flue gas was 7.4-7.7% CO<sub>2</sub>, 14.6% H<sub>2</sub>O, ~ 4.45% O<sub>2</sub>, 200-300 ppm CO, 60-70 ppm NO<sub>x</sub>, and 73-74% N<sub>2</sub>. The composition of the coal-fired flue gas was 12.5-12.8% CO<sub>2</sub>, 6.2% H<sub>2</sub>O, ~ 4.4% O<sub>2</sub>, 50 ppm CO, 420 ppm NO<sub>x</sub>, 420 ppm SO<sub>2</sub>, and 76-77% N<sub>2</sub>. In a typical adsorption/desorption process, about 30 g of the adsorbent was placed in the central part of a stainless steel adsorption column (O.D., 2'; I.D., 1.7'). The adsorbent was pressed to 18-35 mesh. The top and the bottom of the adsorption column were filled with alumina (~170 g) to decrease the dead volume in the separation system. The adsorption column was heated up to 100 °C in a helium atmosphere at a flow of 5 l/min and held at that temperature until there was no CO<sub>2</sub> detected in the effluent gas. The temperature was then adjusted to 80±10 °C and the flue gas mixture was introduced at 5-6 l/min. Generally, the adsorption was carried out for 300-600 seconds. After adsorption, the gas was switched to helium at a flow rate of 5 ml/min to perform the desorption at the same temperature. The time for desorption was 300-600 seconds. The flow rate of the effluent gas was measured by a rotameter. The concentration of CO<sub>2</sub>, O<sub>2</sub>, CO, SO<sub>2</sub> and NO<sub>x</sub> in the effluent gas was measured on-line using a model NGA 2000 non-dispersive infrared CO<sub>2</sub> analyzer; a model NGA 2000 paramagnetic oxygen analyzer; a model NGA 2000 non-dispersive infrared CO analyzer; a model 890 ultraviolet SO<sub>2</sub>

analyzer; and a model NGA 2000 chemiluminescence NO<sub>x</sub> analyzer (Rosemount Analytical, Inc.). The analysis was carried out every 5-6 seconds. (Note that the on-line analysis of the effluent gas composition was carried out after removing the water vapor in the gas mixture. Therefore, the measured gas concentrations were slightly higher than those in the real gas mixture.) Since the alumina also adsorbed the gases, a blank separation test with the column filled only with the alumina (~210 g) was carried out. Therefore, adsorption/desorption capacity of the “molecular basket” adsorbent can be calculated by subtracting the adsorption/desorption capacity between the adsorption experiment and the blank experiment. The adsorption/desorption capacity was calculated from the mass balance before and after the adsorption. The separation factor was defined as the mole ratio of the gases adsorbed over the mole ratio of the gases in the feed.

## Results and Discussions

### 1. Adsorption separation of gas-fired flue gas

Typical CO<sub>2</sub> breakthrough curves for the “molecular basket” adsorbent and the “blank” alumina are shown in Figure 1 for the gas-fired flue gas. Clearly, both the alumina and the “molecular basket” adsorbent can adsorb CO<sub>2</sub>. However, the adsorption performance of the “molecular basket” adsorbent was much better than that of the alumina. The lowest CO<sub>2</sub> emission concentration was ~ 0.8% for alumina and was less than 0.1% for the “molecular basket” adsorbent. The CO<sub>2</sub> adsorption capacity was 1.1 ml (STP)/g adsorbent for the alumina and 26 ml (STP)/g adsorbent for the “molecular basket” adsorbent. In addition, the “molecular basket” adsorbent showed a better selectivity. The “molecular basket” adsorbent did not adsorb O<sub>2</sub>, N<sub>2</sub> and CO, while the CO<sub>2</sub>/O<sub>2</sub> selectivity was 3.5 for alumina. The “molecular basket” adsorbent adsorbed more NO<sub>x</sub> than the alumina. The NO<sub>x</sub> adsorption capacity was 0.0505 ml (STP)/g adsorbent for the “molecular basket” adsorbent and 7.5\*10<sup>-4</sup> ml (STP)/g adsorbent for the alumina. The selectivity of CO<sub>2</sub>/NO<sub>x</sub> was 0.45 for the “molecular basket” adsorbent. However, very little NO<sub>x</sub> was adsorbed before CO<sub>2</sub> breakthrough. The CO<sub>2</sub> and NO<sub>x</sub> adsorption capacity before CO<sub>2</sub> breakthrough was 21 ml (STP)/g adsorbent and 7.1\*10<sup>-3</sup> ml (STP)/g adsorbent, respectively. Therefore, the selectivity of CO<sub>2</sub>/NO<sub>x</sub> was 2.5. Further, while CO<sub>2</sub> was completely desorbed, very little NO<sub>x</sub> desorbed.

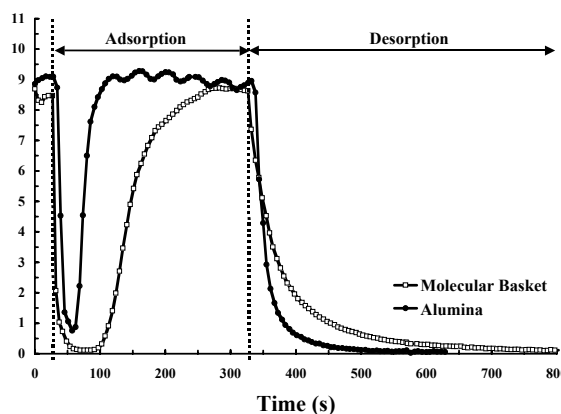
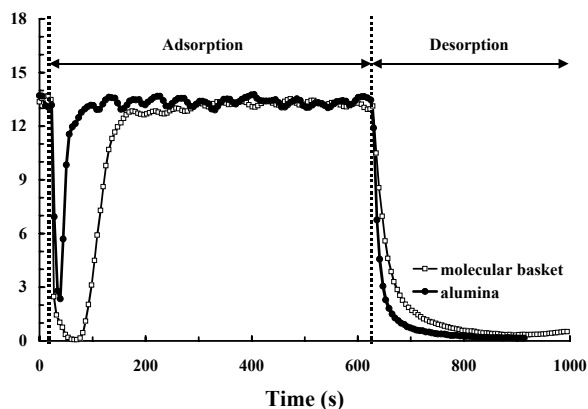


Figure 1 Breakthrough curve of CO<sub>2</sub> for the gas-fired flue gas.

### 2. Adsorption separation of coal-fired flue gas

The adsorption separation of CO<sub>2</sub> from a coal-fired flue gas was also investigated. In the coal fired flue gas, there was a significant concentration of SO<sub>2</sub>. The CO<sub>2</sub> breakthrough curves are shown in Figure 2. Similar trends as for the gas-fired flue gas were observed

for the coal-fired flue gas. The adsorption of  $N_2$  or  $O_2$  by the “molecular basket” adsorbent was below the detection limit of the apparatus. The adsorption capacity for  $CO_2$ ,  $SO_2$  and  $NO_x$  were 36, 0.11 and 0.21 ml (STP)/g adsorbent, respectively. The separation selectivity for  $CO_2/SO_2$  and  $CO_2/NO_x$  was 1.07 and 0.57, respectively. The adsorption capacity for  $CO_2$ ,  $SO_2$  and  $NO_x$  before  $CO_2$  breakthrough was 24, 0.0074 and 0.028 ml (STP)/g adsorbent, respectively. Therefore, the separation selectivity for  $CO_2/SO_2$  and  $CO_2/NO_x$  was 10.7 and 2.86, respectively, before  $CO_2$  breakthrough. Again, while the desorption of  $CO_2$  was complete, very little  $NO_x$  and  $SO_2$  desorbed.



**Figure 2** Breakthrough curve of  $CO_2$  for the coal-fired flue gas.

Compared with the  $CO_2$  adsorption capacity in the simulated flue gas condition, the  $CO_2$  adsorption capacity in the power plant flue gas condition was about ~30% lower. The adsorption capacity for the coal-fired flue gas was 36 ml (STP)/g adsorbent at  $80 \pm 10$  °C with the feed composition of 12.5-12.8%  $CO_2$ , ~4.4%  $O_2$ , 50 ppm CO, 420 ppm  $NO_x$ , 420 ppm  $SO_2$ , 6.2%  $H_2O$  and 76-77%  $N_2$ . The adsorption capacity for the simulated flue gas mixture was 53 ml (STP)/g adsorbent at 75 °C with the feed composition of 13.9%  $CO_2$ , 3.95%  $O_2$ , 6.43%  $H_2O$  and 75.7%  $N_2$ . There are several reasons which may cause the difference in the adsorption capacity. First, the  $CO_2$  concentration in the coal-fired flue gas mixture was lower than that in the simulated flue gas mixture. At lower  $CO_2$  concentrations, the  $CO_2$  adsorption capacity will be lower.<sup>4</sup> Second, the adsorbent with different physical forms will have different  $CO_2$  adsorption capacities. A comparison study on the  $CO_2$  adsorption by a powder adsorbent and by a pellet (18-35 meshes) adsorbent was carried out and the results are shown in Figure 3. It is clearly shown in Figure 3 that the pellet adsorbent had a lower  $CO_2$  adsorption capacity than the powder adsorbent. The adsorption capacity of the pellet adsorbent was about 10% lower than that of the powder adsorbent. Third, the higher flow rates in the power plant flue gas separation tests resulted in the lower adsorption capacity. The feed flow rate was 167ml/min.g adsorbent in the power plant flue gas separation tests and was only 5 ml/min.g adsorbent in the simulated flue gas separation. Lastly, minor gas components, i.e.,  $NO_x$  and  $SO_2$ , influenced the adsorption of  $CO_2$ . Since  $NO_x$  and  $SO_2$  are acid gases and the adsorbent is basic in nature, the  $NO_x$  and  $SO_2$  are competitive adsorbates for  $CO_2$ . Our experimental results showed that the adsorption of  $NO_x$  by the “molecular basket” adsorbent was even stronger than that of  $CO_2$  in some experimental conditions. The pre-removal of  $NO_x$  and  $SO_2$  from the flue gas mixture is therefore preferred for the adsorption separation of  $CO_2$  from the flue gas mixture by this “molecular basket” adsorbent.

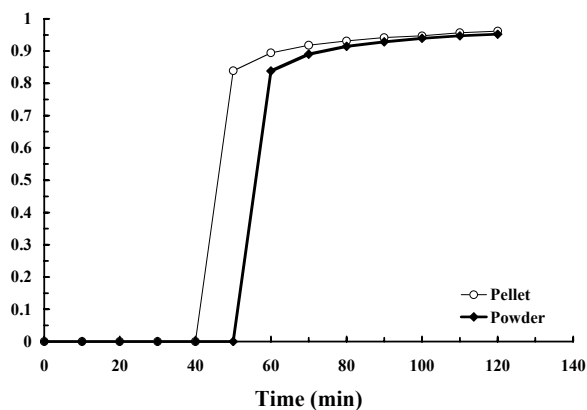


**Figure 3** Comparison of the  $CO_2$  breakthrough curve of the “molecular basket” adsorbent in pellet and in powder form. Operation condition: Weight of adsorbent: 2.0 g; Feed composition: 14.9%  $CO_2$ , 4.25%  $O_2$  and 80.85%; Temperature: 75 °C; Feed flow rate: 10 ml/min.

## Conclusions

$CO_2$  can be selectively separated from the flue gases of power plant by using the novel “molecular basket” adsorbent MCM-41-PEI-50. The adsorbent hardly adsorbs any  $N_2$ ,  $O_2$  and CO. The selectivity of  $CO_2/NO_x$  was 2.5 for gas-fired flue gas and the selectivity of  $CO_2/SO_2$  and  $CO_2/NO_x$  were 10.7 and 2.86 for coal-fired flue gas, respectively. Very little  $NO_x$  and  $SO_2$  desorbed after adsorption indicating the need for pre-removal of  $NO_x$  and  $SO_2$  from the flue gas before capture of  $CO_2$  by the PEI based “molecular basket” adsorbent.

**Acknowledgement.** Funding for the work was provided by the U.S. Department of Defense (via an interagency agreement with the U.S. Department of Energy) and the Commonwealth of Pennsylvania under Cooperative Agreement No. DE-FC22-92PC92162.

## References

- (1) Maroto-Valer, M. M.; Song, C.; Soong, Y. (Eds). Environmental Challenges and Greenhouse Gas Control for Fossil Fuel Utilization in the 21<sup>st</sup> Century. Kluwer Academic/Plenum Publishers, New York, **2002**, 447 pp.
- (2) Song, C.; Gaffney, A. M.; Fujimoto, K. (Eds).  $CO_2$  Conversion and Utilization. American Chemical Society (ACS), Washington DC, ACS Symp. Series, Vol. 809, **2002**, 448 pp.
- (3) U.S. Department of Energy, Carbon Sequestration-Research and Development, **1999**, [http://www.fe.doe.gov/coal\\_power/sequestration/reports/rd/index.html](http://www.fe.doe.gov/coal_power/sequestration/reports/rd/index.html).
- (4) Xu, X.C.; Song, C.; Andresen, J.M.; Miller, B.G.; Scaroni, A.W., Energy & Fuels, **2002**, 16, 1463-1469.
- (5) Xu, X.C.; Andresen, J.M.; Song, C.S.; Miller, B.G.; Scaroni, A.W. Am. Chem. Soc., Div. Fuel Chem., **2002**, 47 (1), 67-68.
- (6) Xu, X.C.; Song, C.; Andresen, J.M.; Miller, B.G.; Scaroni, Proceeding of the Nineteenth Annual International Pittsburgh Coal Conference, September 23-27, **2002**, Pittsburgh, PA USA. (Paper No. 39-2)

## Performance of Solid Amine Sorbents

M. L. Gray<sup>1\*</sup>, Y. Soong<sup>1</sup>, K. J. Champagne<sup>1</sup>, H. Pennline<sup>1</sup>, J. Baltrus<sup>1</sup>,  
R.W. Stevens, Jr.<sup>2</sup>, R. Khatri<sup>2</sup>, S. S. C. Chuang<sup>2</sup>, and S. Khan<sup>3</sup>

<sup>1</sup>US Department of Energy, National Energy Technology Laboratory, P.O. Box 10940, Pittsburgh, PA, 15236. [Gray@NETL.DOE.GOV](mailto:Gray@NETL.DOE.GOV). (412) 386-4826, Fax (412) 386-4808.

<sup>2</sup>Chemical Engineering Department, University of Akron, Akron, OH, 44325-3906.

<sup>3</sup>Chemistry and Biochemistry Department, Duquesne University, Pittsburgh, PA, 15282

### ABSTRACT

Solid amine sorbents have been successfully prepared by reacting oxygen rich substrates with alkoxy amine compounds. The initial solid sorbents have been proven to be competitive with existing environmental CO<sub>2</sub> controlled life sorbents. It was determined that both silicon and titanium based substrates were very reactive with these alkoxy amine compounds resulting in stable solid amine sorbents. XPS analysis has indicated that the amine group was incorporated onto the surface of these substrates in the range of 3-7 percent. The performance of these silicon and titanium amine sorbents will be described within this paper.

**Keywords:** carbon dioxide, capture, and amine sorbent.

### INTRODUCTION

The concentration of CO<sub>2</sub> in our atmosphere is promoted by the combustion of fossil fuels for the generation of electricity. Capturing CO<sub>2</sub> from flue-gas streams is an essential parameter for the carbon management for sequestrating of CO<sub>2</sub> from our environment. Current technologies<sup>1</sup> being considered for CO<sub>2</sub> sequestration include: disposal of CO<sub>2</sub> in deep oceans; depleted oil and gas fields; deep saline formations (aquifers); and recovery of enhanced oil, gas, and coal-bed methane. However, the current cost for the utilization of these types of technologies has proven to be too expensive. Consequently, reducing the cost for the capture of CO<sub>2</sub> will be a critical step in the overall carbon management program.

The physical and chemical adsorption of CO<sub>2</sub> can be achieved by using solvents, cryogenic techniques, membranes, and solid sorbents. The large-scale operation of these technologies is energy intensive when applied to capturing CO<sub>2</sub> in dilute stream, such as flue gas, which consist of 15% CO<sub>2</sub> by volume for most coal combustion systems. Amine-based, solvent-capture systems are the most energy efficient option, but are energy intensive due to the large amount of water needed in these system. Excessive water is required because of the corrosion and air flow problems created by the use of monoethanolamine (MEA), diethanolamine (DEA), or methyl-diethanolamine (MDEA) in these aqueous-based, CO<sub>2</sub>-capture systems. The proposed reaction sequences for using primary, secondary, and tertiary alkanolamines reacting with dissolve CO<sub>2</sub> are shown below.

Solid-amine CO<sub>2</sub> sorbents should have similar reactions with

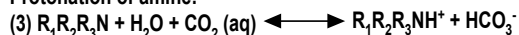
Formation of the zwitterion ion:



Formation of amine carbamate:



Protonation of amine:



airborne CO<sub>2</sub>, water vapor, and the amine functional group on its surface. Consequently, these types of sorbents are being used in aircraft, submarine, and spacecraft technologies<sup>2-4</sup>. However, the cost of these sorbents is too expensive for large-scale applications in the utility industry. Consequently, the development of economical amine-enriched sorbents based on reacting oxygen rich substrates with alkoxy amine compounds will be discussed within this paper.

### EXPERIMENTAL PROCEDURES:

**Samples**-- The three alternative oxygen rich solid substrates that were examined as CO<sub>2</sub> capture sorbents were a Tetraethyl orthosilicate (SBA-15) from Aldrich Chemical Company, a Titanium (II) oxide (TiO-1) from Aldrich Chemical Company and a Immobilized amine sorbent (IAS) from an leading industrial manufacturer.

**Amine Treatment Process**--The actual conditions for incorporating the amine group into the structure of the oxygen rich substrates will not be discussed in this paper due to pending patent applications.

**CO<sub>2</sub> Capture Capacity**--The chemical CO<sub>2</sub> capture capacities were determined by the combination of Temperature Programmed Desorption (TPD) and Mass Spectroscopy (MS) analyses. The adsorption of CO<sub>2</sub> was achieved in the presence of moisture at 25 °C and the total desorption of CO<sub>2</sub> was achieved over the temperature range of 30 – 60 °C. The composition of the experimental gas stream used in these test runs was 10% CO<sub>2</sub>/H<sub>2</sub>O/He. The detailed operating conditions for this procedure were previously described in the literature<sup>5</sup>. The experimental set-up for these test runs is shown in figure 1.

**XPS Analysis** – The amount of nitrogen of the surface of the amine-enriched sorbent was determined by XPS analysis. The details of this experimental procedure have been reported in the literature<sup>6</sup>.

### RESULTS AND DISCUSSION:

Initially, the performance of the prepared amine-enriched sorbents (SBA-15 and TiO-1) were compared to the existing industrial solid amine sorbent (IAS). These sorbents were place in a 10% CO<sub>2</sub>/H<sub>2</sub>O/He stream and TPD, and MS analyses were conducted determined the performance of these CO<sub>2</sub> capture sorbents. The adsorption/desorption of CO<sub>2</sub> for these sorbents were determined over the temperature range of 25 – 60 °C. A typical TPD/MS spectra are shown in figures 2. According to the TPD/MS analysis, all of the sorbent were successful in the capture of CO<sub>2</sub> the moist experimental gas streams. The comparison of the CO<sub>2</sub> capture performances and XPS results for these sorbents are summarized in Table 1.

**Table 1: TPD CO<sub>2</sub> Desorption and XPS Data of the Amine-Enriched Sorbents**

| Sorbents | XPS %Nitrogen | μmol/g CO <sub>2</sub> Captured |
|----------|---------------|---------------------------------|
| IAS      | 6.68          | 1886.6                          |
| SBA-15   | 7.13          | 2011.4                          |
| TiO-1    | 3.59          | 1057.2                          |

As shown in Table 1, the best performing sorbent for the capture of CO<sub>2</sub> from these experimental gas streams was SBA-15. With the surface nitrogen value of 7.13 % the total amount of CO<sub>2</sub> captured was 2011.4 μmol/g for the SBA-15 sorbent. The SBA-15 performed slightly better then the IAS sorbent (1886.6 μmol/g) which may indicate that there are potential applications within in the

environmental control CO<sub>2</sub> capture industry for the SBA-15 sorbent. The TiO-1 was least reactive with the alkoxy amine compounds resulting in lower a CO<sub>2</sub> capture capacity of 1057.2 μmol/g with a surface nitrogen value of 3.59%. The overall performance for these sorbents will be determined by multiple regeneration testing (5-10 recycle runs) and these results will be disclosed in future publications.

## CONCLUSION

Preliminary results indicate that the SBA-15 sorbent is comparable to the IAS sorbent which is currently being used environmental CO<sub>2</sub> controlled life sorbent. Additional experimental work is now underway to improve the performances of the SBA-15 and TiO-1 as CO<sub>2</sub> capture sorbents.

## REFERENCES

1. DOE Report Doe/ER-30194, "Research Needs Assessment for the Capture, Utilization and Disposal of Carbon Dioxide from Fossil Fuel-Fired Power Plants," 1993.
2. US Patent 4,810,266, Zinnen, H. A., Oroskar, A. R., and Chang, C. H. "CO<sub>2</sub> Removal using Aminated Carbon Molecular Sieves," 1989.
3. US Patent 5,492,683, Bibara P.J., Naletta T. A. "Regenerable Support Amine Polyol Sorbent," 1996.
4. US Patent 5,876,488, Bibara P. J. Filburn T. P., Nalette T. A. "regenerable Solid Amine Sorbent," 1999.
5. Soong, Y., Gray, M. L., Siriwardane, R. V., Champagne, K. J., Stevens, Jr., R. W., Toochinda, P., and Chuang, S. S. C. "Novel Amine Enriched Solid Sorbents for Carbon Dioxide Capture," Fuel preprint, 46 (1), pp. 285, 2001.
6. Gray, M. L., Champagne, K. J., Soong, Y., Killmeyer, R. P., Baltrus, J., Maroto-Valer, M. M., Andersen, J. M., Ciocco, M.V., and Zandhuis, P.H., ACS Chapter Book, "Environmental Challenges and Greenhouse Gas Control for Fossil Fuel Utilization in the 21 st Century", unpublished.

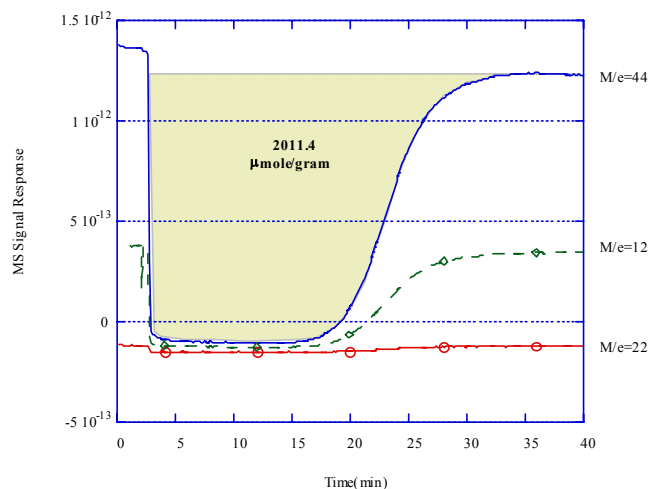


Figure 2: Typical TPD Mass spectra of SBA-15

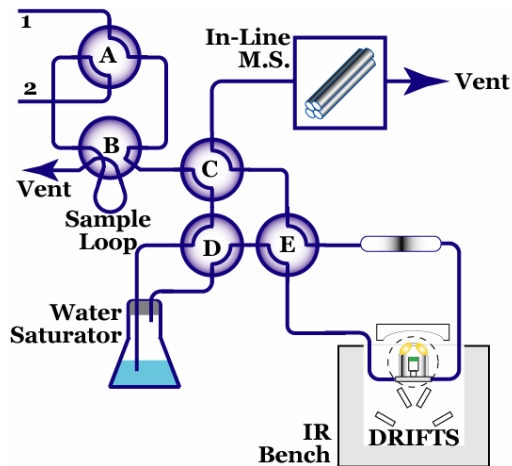


Figure 1: Experimental set-up for TPD/MS analysis

## Development of a CO<sub>2</sub> Affinity Ceramic Membrane

*R. J. Ciora, Jr. and P. K.T. Liu*  
Media and Process Technology Inc.  
1155 Willaim Pitt Way, Pittsburgh, PA 15238  
*T. T. Tsotsis, and M. Sahimi*  
Department of Chemical Engineering  
University of Southern California  
Los Angeles, CA 90089-1211

### Significance of A CO<sub>2</sub> Affinity Ceramic Membranes

Most CO<sub>2</sub> selective membranes available today can effectively separate CO<sub>2</sub> from combustion off-gas at low temperatures. However, these membranes are not ideal for CO<sub>2</sub> sequestration applications due to (i) the large volume of off-gas that must be processed and (ii) the low partial pressure available in these streams. One way to overcome these intrinsic barriers associated with the use of membrane technology is to separate CO<sub>2</sub> in-situ from the coal gasification off-gas after shift reaction while producing high pressure hydrogen as clean fuel. Thus, the membrane can be used on a stream with a significantly reduced volume at a high pressure. In this presentation we will discuss one of the membrane concepts we are developing: a CO<sub>2</sub>-affinity ceramic membrane, which can be used to selectively remove CO<sub>2</sub> from the high temperature stream (e.g., 200 to 400°C).

### Characterization of Membrane Material

The material selected as a candidate for the CO<sub>2</sub> selective membrane has been evaluated comprehensively to insure its adequacy as a membrane material. Here we present the characterization results from TG/MS, DRIFTS and cyclic adsorption/desorption to demonstrate its reversibility with respect to its affinity to CO<sub>2</sub>. The TG study indicates that significant weight loss from the 25°C to 600°C. However, according to MS, CO<sub>2</sub> weight loss is not significant until ~200°C. Further, the majority of the weight loss takes place at <400°C. To determine its degree of reversibility, we also performed cyclic adsorption and desorption studies using TGA for the temperature ranging from 200 to 350°C. The result shows that a majority of the CO<sub>2</sub> loss is reversible. It appears that the degree of reversibility begins to stabilize after the 5<sup>th</sup> cycle. Cyclic adsorption/desorption greater than the 5<sup>th</sup> cycle is presently underway. DRIFTS was performed to characterize the surface change as a result of CO<sub>2</sub> adsorption/desorption. Its trend is consistent with that determined by TGA.

### Membrane Synthesis – Preliminary Experimental Results

Several methods have been under investigation for the synthesis of the proposed CO<sub>2</sub>-affinity membrane. Some preliminary results obtained from slip casting, one of the methods currently explored by us, are presented here. Slip casting is a common method employed to prepare micro porous membranes with the pore size ranging from ~40Å to microns. To successfully develop a membrane through this approach, a homogenous solution suspended with particles with appropriate size is a prerequisite. In addition, the slip viscosity and the casting time, and many other parameters are important. SEM examination of the unsupported film shows that we are able to prepare a slip with the particles size in the range of 0.03 to 0.05 micron. Figure 1 presents one of the membranes prepared via slip casting. It is clear that a nearly defect free nanoporous membrane has been prepared with this CO<sub>2</sub>-affinity ceramic material. Its pore size is estimated in the range of ~100Å in comparison with the reference Al<sub>2</sub>O<sub>3</sub> membrane with a pore size of ~100Å shown in Figure 2.

Presently, we are actively pursuing the use of the CVD/I technique to plug the openings of this porous membrane as a post treatment. Thus, CO<sub>2</sub> can selectively permeate through the thin film formed by the selected CO<sub>2</sub>-affinity material. This CVD/I technique has been successfully employed by us to seal the commercial 100Å Al<sub>2</sub>O<sub>3</sub> membrane to become a nearly non-porous membrane with an ultra thin layer in the range of <1.5 micron. We anticipate this technique can be used here for the same purpose.

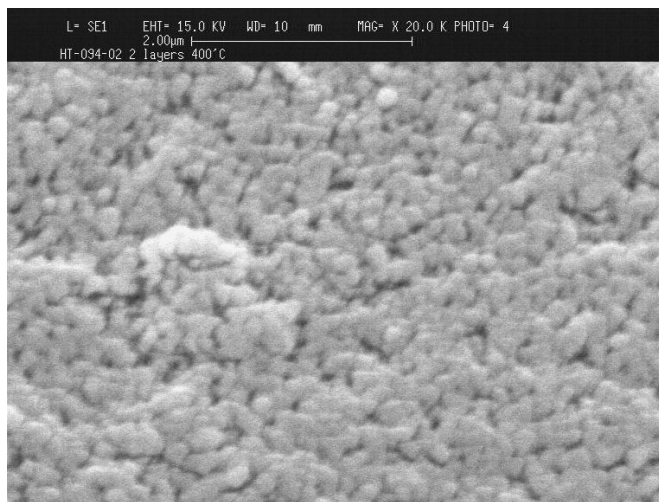


**Figure 1** SEM photomicrograph of the porous ceramic membrane prepared with the CO<sub>2</sub>-affinity material via slip casting.

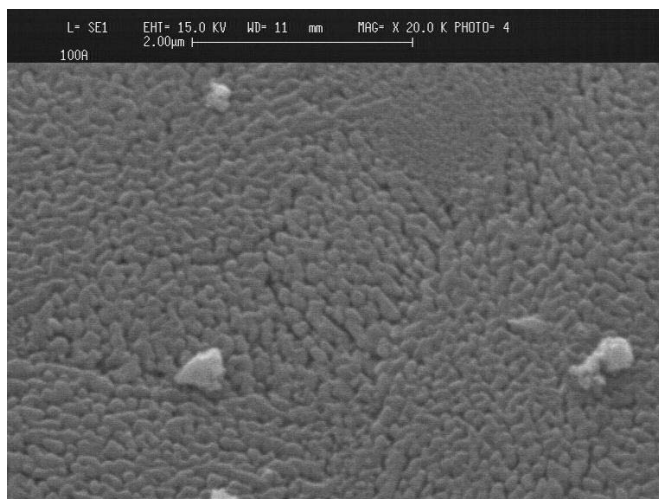


**Figure 2** SEM photomicrograph of commercial Al<sub>2</sub>O<sub>3</sub> membrane with 100Å pore size.

# NEW AMINES FOR CARBON DIOXIDE SEPARATION FROM GAS-MIXTURES

Angela Dibenedetto\*, Michele Aresta and Roberta Girardi

Department of Chemistry and METEA Research Center, University of Bari, Campus Universitario, 70126, Bari – Italy.  
E-mail: a.dibenedetto@chimica.uniba.it

## Introduction

Mono- and di-amines have been used for carbon dioxide separation from gas mixtures. Derivatized diamines bearing a silyl-group have been shown to pick-up one mol of CO<sub>2</sub> per mol of amine, affording intra-molecular carbamates that reversibly release carbon dioxide. The silyl-diamines can be converted into xerogels that are able to adsorb carbon dioxide. The absorption-desorption curves show a good efficiency in CO<sub>2</sub> up-take, that is higher than that of monoamines[1,2] in the same conditions.

## Results and Discussion

It is well established that aliphatic amines react with carbon dioxide to afford ammonium carbamates as represented in Eq. 1.



In this work we have studied the up-take of carbon dioxide using aliphatic di-amines (H<sub>2</sub>N(CH<sub>2</sub>)<sub>2</sub>NH(CH<sub>2</sub>)<sub>3</sub>Si(OMe)<sub>3</sub> I and CH<sub>3</sub>(CH<sub>2</sub>)<sub>2</sub>NH(CH<sub>2</sub>)<sub>2</sub>NH<sub>2</sub> II) and found that they are able to capture 1 mol of CO<sub>2</sub> per mol of amine. Their behavior has been compared with that of monoethanolamine (MEA), used at industrial level, in the same reaction conditions.

Figure 1 shows the up-take curve by di-amines I and II, and that of MEA.

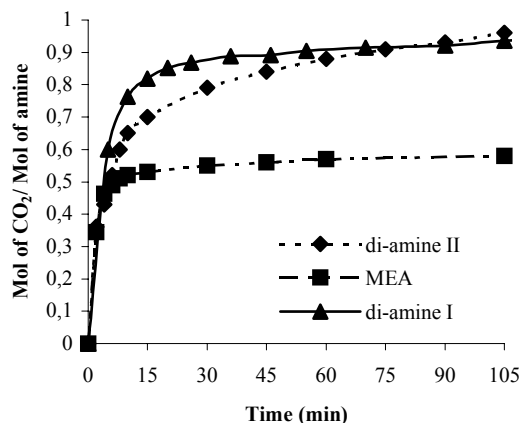


Figure 1. CO<sub>2</sub> up-take of diamines comparing with MEA.

Differently from MEA, one mol of CO<sub>2</sub> per mol of amine was up-taken by amines I and II. This behaviour has been explained considering that, as described in a previous work [3], the amine I affords an intra-molecular carbamate. The reaction was quite fast (less than 20 minutes) and a glassy material difficult to handle was isolated. Nevertheless, by evaporating directly on a single KBr disk the amine solution under CO<sub>2</sub> atmosphere, it was possible to record the IR spectrum which showed the characteristic band at 1540 cm<sup>-1</sup> due to the carbamate RHNCOO<sup>-</sup> moiety [3]. Moreover, the <sup>1</sup>H and <sup>13</sup>C NMR

spectra of a solution of the amine I under 0.1 MPa of CO<sub>2</sub> confirm the formation of the intra-molecular carbamate.

As shown in Fig. 1, also di-amine II takes-up CO<sub>2</sub> with a 1:1 molar ratio, but, differently from amine I, affords a white light powder more easy to handle.

In both cases, the absorption was reversible and carbon dioxide was completely released at 333 K. In fact, if neat amine was used, the starting material was quantitatively recovered.

Following such discovery, we built a laboratory apparatus to follow the carbon dioxide absorption and desorption using either the neat amines, or their water- or organic solvent-solutions. The absorption/desorption curve when free amine I was placed in contact with a gas mixture (14% of CO<sub>2</sub>) is shown in Figure 2.

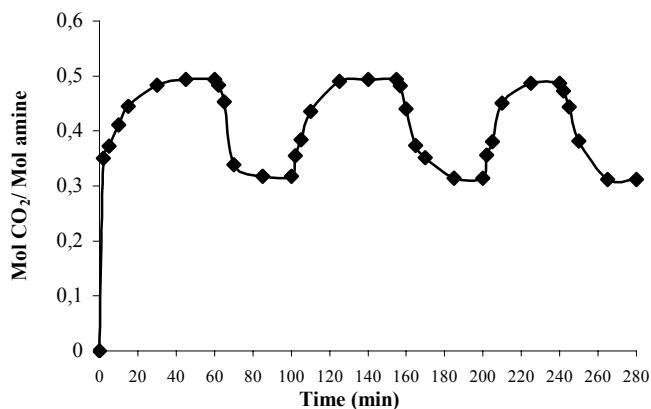


Figure 2. CO<sub>2</sub> absorptio/desorption curve for neat amine I

As Figure 2 shows after few minutes di-amine I was able to up-take carbon dioxide with a 1:1 molar ratio at room temperature. By heating to 333 K, half of the CO<sub>2</sub> absorbed was released. Such amount was then absorbed and desorbed for several cycles (Fig. 2). Most probably the working temperature range is limiting the release of carbon dioxide. The upper limit of the temperature is given by either the use of water or organic solvents or by the vapour pressure of the amine and its thermal stability.

For avoiding losses, we have tried to change the state of the di-amine I from liquid to solid and have transformed the liquid di-amine into a xerogel. The silica xerogel was obtained by condensation of amine I and silicon alkoxydes under hydrolytic conditions.

By using the solid species, the desorption was carried out at temperature higher than that of liquid amine increasing the efficiency of the desorption.

In fact, as shown in Figure 3, the xerogel was able to absorb and desorb CO<sub>2</sub> from a gas mixture in a very short time and for several cycles in a batch system.

Studies are in progress for elucidating how the amine is linked to the silicon alkoxydes in the xerogel and its structure. The next step will be the design of a flow system.

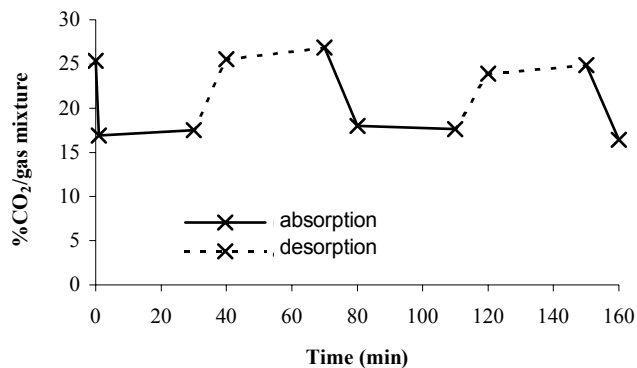


**Figure 3.** Carbon dioxide absorption/desorption cycles by using diamine I in a xerogel

### Conclusions

The use of di-amines for the reversible uptake of carbon dioxide is more efficient than the use of monoamines. In fact, di-amines uptake twice the amount of carbon dioxide per mol from a gas mixture at 0.1 MPa total pressure (14% CO<sub>2</sub>). Moreover, the di-amines converted into a xerogel are more efficient than liquid amines or amine solutions in water or organic solvents for capturing CO<sub>2</sub> from a gas mixture. They can be reused for several cycles and the working temperature is higher than that of free amines.

**Acknowledgement.** The financial support by MIUR, Project n° 9803026360 and n° MM03027791 are acknowledged.

### References

- (1) Dibenedetto, A., Aresta, M., Narracci, M. 223<sup>rd</sup> ACS National Meeting, April 7-11, 2002, Orlando Florida.
- (2) Michele Aresta and Angela Dibenedetto 6<sup>th</sup> International Conference on Greenhouse Gas Control Technologies (GHGT-6) 30<sup>th</sup> September-4<sup>th</sup> October 2002, Kyoto, Japan, Book of Abstracts CAABP8.
- (3) Dibenedetto, A., Aresta, M., Narracci, M., Fragale, C. *Green Chemistry* 2002, 4, Issue 05, 439-443.

# Sorbent Development for Carbon Dioxide Separation and Capture

Daniel J. Fauth, James S. Hoffman, and Henry W. Pennline

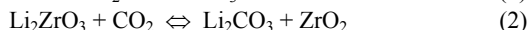
U.S. Department of Energy  
National Energy Technology Laboratory,  
P.O. Box 10940, Pittsburgh, PA 15236

## Introduction

The combustion of fossil fuels emits considerable levels of carbon dioxide, a greenhouse gas proposed to influence global climate warming from human activities. Large stationary sources, such as coal-based electric generating plants, are likely targets for CO<sub>2</sub> capture and sequestration if regulation is deemed necessary for the 21<sup>st</sup> century and beyond. A number of mitigation technologies, to include CO<sub>2</sub> capture and sequestration, are currently under investigation<sup>1-4</sup>. The majority of these processes require CO<sub>2</sub> in a concentrated form.

A wide range of technologies currently available to separate CO<sub>2</sub> from flue gas include chemical absorption with monoethanolamine (MEA), membrane separation, cryogenic fractionation, and adsorption using molecular sieves<sup>5</sup>. It has been generally established that CO<sub>2</sub> capture for most of these processes is expensive and energy-intensive. Hence, a need exists for developing a range of emerging approaches to separate CO<sub>2</sub> with more cost-effective processes. Such a technique for CO<sub>2</sub> capture may employ dry scrubbing – a process that includes chemical absorption with a solid sorbent. Dry, regenerable sorbent processes are cyclic in the sense that a sorbent can remove the pollutant, be regenerated (and in this step yield a concentrated stream of CO<sub>2</sub>), and thus be reused.

The approach undertaken in this study was to investigate the reaction of CO<sub>2</sub> with calcium-based reagents and a number of calcium-based impregnated materials using a thermogravimetric analyzer. The chemical reactions for CO<sub>2</sub> capture using these compounds are illustrated below. The forward reaction pathway depicts absorption of CO<sub>2</sub>, whereas regeneration is expressed as the reverse reaction path.



In the thermogravimetric (TG) system, the change in sample weight was recorded as the sample was exposed to gases under conditions representative of absorption and regeneration. The extent of chemical reaction was linked to sample weight change, from which kinetic rate parameters could be estimated.

## Experimental

An activated alumina (200 m<sup>2</sup>/g) containing lanthanum was obtained from Alcoa Industrial Chemical Division, Vidalia, LA. Lanthanum (3.1 wt%) was added to impart high temperature stability to the alumina. For a given preparation, calcium nitrate tetrahydrate was dissolved in acetone for 1 hour. The alumina support (cylindrical extrudates) was immediately added to the calcium nitrate solution and soaked overnight at room temperature. The mixture was subsequently vacuum filtered and dried at 110°C for 18 hours. Lastly, the calcination step (400°C for up to 48 hours) converted the Ca-based complex into calcium oxide uniformly distributed throughout the carrier as confirmed by SEM-EDX analysis. A CaO loading of 13.8 wt% was determined for the calcined CaO/La<sub>2</sub>O<sub>3</sub>-doped/Al<sub>2</sub>O<sub>3</sub> material.

A number of mesoporous zirconia catalyst supports (Type A and Type B) were purchased from Alfa Aesar. The zirconium oxide substrates were 1/8 inch in diameter having larger pore size and smaller surface area relative to the activated alumina. Both zirconia supports had a bimodal pore diameter distribution. Type A had approximately double the surface area of Type B (90 versus 51 m<sup>2</sup>/g); with Type A having a corresponding smaller pore size for both maximums of the pore size distribution. Elemental analysis performed on the calcined CaO/ZrO<sub>2</sub> materials showed CaO loading to be 6.77% and 5.99% for Type A and Type B, respectively. The physical properties of the activated alumina and zirconia oxide carriers are included in Table 1.

**Table 1. Physical and Chemical Characterization of Alumina and Zirconium Oxide Carriers**

| Ga-200L Alumina<br>(Cylindrical Extrudates) | Analysis of Lot<br>No. G2L0C011 |         |
|---|---------------------------------|---------|
| Surface area (M <sup>2</sup> /g)            | 215                             |         |
| Lanthanum (wt%)                             | 3.1                             |         |
| Pore volume (cc/g)                          | 0.61                            |         |
| Thermal Stability aged 1200°C, 3 hrs.       |                                 |         |
| Surface area (M <sup>2</sup> /g)            | 53                              |         |
| Zirconia Catalyst Support                   | Type A                          | Type B  |
| Pellet diameter (in)                        | 1/8                             | 1/8     |
| Surface area (M <sup>2</sup> /g)            | 90                              | 51      |
| Median pore diameter, bimodal<br>(Angstrom) | 80/400                          | 160/600 |
| Total pore volume (cc/g)                    | 0.31                            | 0.30    |
| Percent purity (metal basis)                | 99.8                            | 99.8    |

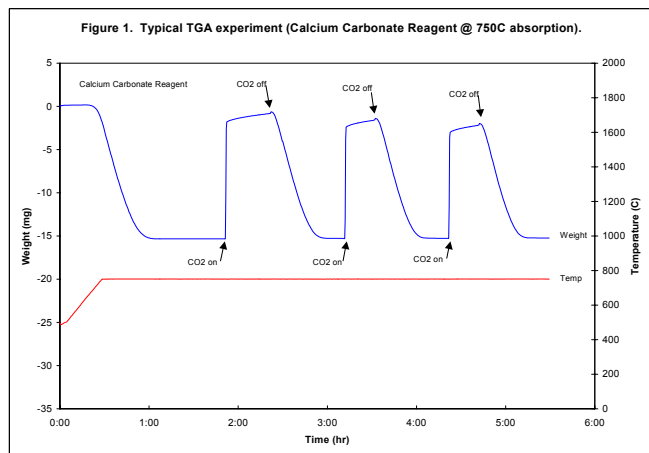
Thermogravimetric experiments were performed using a microbalance assembly consisting of a Cahn TG-131 Thermogravimetric Analyzer (TGA). A gas cylinder supplied carbon dioxide of stock gas grade (99.99%) to the TGA unit. In a representative test, ~200 mg of sample was initially charged into a quartz sample pan. Slotted apertures in the bottom and sidewall of the sample pan were added to help mitigate gas diffusional resistance. A type K thermocouple located directly below the suspended sample measured and controlled the internal temperature within the thermogravimetric assembly. A gas flow rate of 140 cc/min was employed for all tests. Prior to CO<sub>2</sub> absorption, each sample was preconditioned and dried in nitrogen elevating the reactor temperature to 150°C, followed by subsequent heating to achieve the absorption temperature of interest (typically 500-750°C). Upon achieving steady state in dry nitrogen, the introduction to carbon dioxide was made. A constant CO<sub>2</sub> flow rate of 140 cc/min. was maintained. The CO<sub>2</sub> absorption stage was allowed to proceed until a steady-state weight gain was achieved, or it was otherwise halted if excessive duration of time was required to reach steady state.

## Results and Discussion

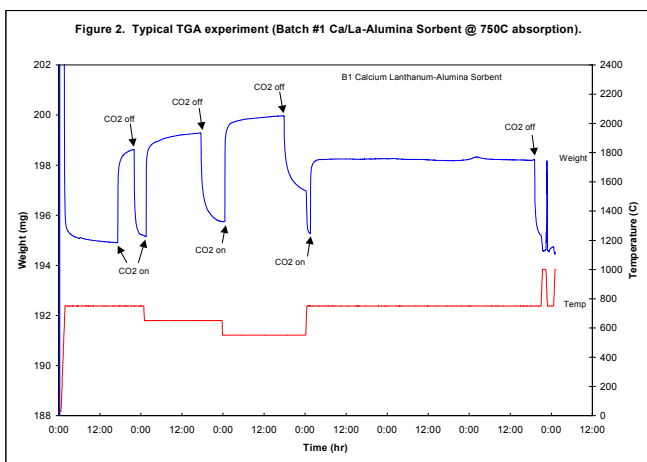
Calcium-Based Reagents: To help elucidate the chemical behavior of the active metal within the impregnated sorbent, several tests were conducted using pure reagent compounds (CaO, CaCO<sub>3</sub>). The CO<sub>2</sub> absorption reaction was initially very fast (50% theoretical conversion after an hour), followed by much slower reaction. The absorption reaction appeared favorable between 750-850°C, while regeneration was attainable at 1000°C. By raising the temperature from 850°C to 1000°C in N<sub>2</sub>, the calcium-based reagents could be rapidly regenerated within a short period of time (~15 minutes). Thermal regeneration of the product was strongly dependent on the background gas composition. In nitrogen, the

regimes of temperature suitable for regeneration was found to be significantly lower than in pure CO<sub>2</sub>. For example, CaCO<sub>3</sub> began to decompose at 650°C in nitrogen, whereas in CO<sub>2</sub> it was relatively stable up to 900-950°C.

A multi-cycle test with repeated absorption and regeneration steps was conducted at 750°C starting with CaCO<sub>3</sub> (**Figure 1**). Gas composition was switched between carbon dioxide (absorption) and nitrogen (regeneration) at 30-minute increments, resulting in one-hour intervals for a complete cycle. Although the cycles appear very similar, a slight degradation in performance was apparent. For equivalent cycle times, the CO<sub>2</sub> capture (conversion to calcium carbonate) decreased by ~2 percentage points, from 36% to 34% to 32% over 3 cycles. Gupta<sup>6</sup> observed slight degradation of CaCO<sub>3</sub> reagent over a 3-cycle test.



**Ca-based/La-modified/Alumina Sorbent:** Absorption tests with the Ca-based lanthanum-doped alumina sorbent were performed upon exposure to pure CO<sub>2</sub> at temperatures between 500-750°C (**Figure 2**). The alumina substrate, when tested individually at temperatures between 650-850°C in pure CO<sub>2</sub>, showed no appreciable affinity to sorb CO<sub>2</sub>. As with calcium-based reagent tests, the initial rate of reaction is very fast, achieving 15-20% sorbent conversion for the CaO/La<sub>2</sub>O<sub>3</sub>/Al<sub>2</sub>O<sub>3</sub> material. However, the reaction slows significantly and enters a regime characterized by very long residence time required to achieve minimal increase in sorbent conversion. This regime was partially attributed to increased gas diffusional resistance through a product layer of calcium carbonate.



**Calcium-based/Zirconia Sorbent:** Thermogravimetric testing of the prepared calcium deposited on zirconium oxide substrates were performed at 500°C in pure CO<sub>2</sub>. Type A and Type B zirconia carriers, with no calcium deposition, showed a slight weight gain indicating some CO<sub>2</sub> absorption was achieved. However, upon gas switching to N<sub>2</sub>, the carriers lost all of the gained weight. It is logical to assume that the captured CO<sub>2</sub> was not due to chemical reaction to form carbonate, but rather another mechanism.

Similar to the calcium reagents and the CaO/La<sub>2</sub>O<sub>3</sub>/Al<sub>2</sub>O<sub>3</sub> sorbent tests, the absorption reaction was initially rapid and then entered into a slower kinetic regime. However, the zirconia sorbents performed much better, as characterized by the much higher conversion attained versus the CaO/lanthanum-doped alumina sorbent. Conversions ranging from 50-75% were observed for the Ca/zirconia sorbents versus 15-20% conversion for the CaO/lanthanum-doped alumina sorbent. One obvious explanation for the improved conversion was attributed to the pore size differential between mesoporous zirconia and microporous lanthanum-alumina. Even though the alumina had a higher surface area, pore pluggage and/or increased diffusional resistance through the calcium carbonate product layer appeared to be a plausible cause for the less active calcium/alumina sorbent.

The permanence of the sequestered CO<sub>2</sub> onto the Ca/zirconia sorbents was also in stark contrast to the alumina sorbents. The Ca/zirconia materials exhibited significantly less weight loss and retained a larger fraction of the absorbed CO<sub>2</sub> upon gas switching from pure CO<sub>2</sub> to N<sub>2</sub> at the end of the absorption stage at 500°C. Approximately 70-80% of the sorbed CO<sub>2</sub> remained with the sorbent for the Type B zirconia (larger pore volume and smaller surface area) and roughly half of the sorbed CO<sub>2</sub> with the sorbent for the Type A zirconia. Regeneration of the Ca/zirconia sorbents was quickly achieved by elevating the temperature from 500°C to 750°C under nitrogen.

## Conclusion

Dry, regenerable sorbent processes capable of removing carbon dioxide from point generation sources can be used for the capture of CO<sub>2</sub>. Cyclic reaction performances of various Ca-based sorbents were investigated using a thermogravimetric analyzer. Incorporating the materials at temperatures expected to be seen under gasification conditions, pure calcium and calcium/alumina systems had good initial reactivity, but the capacity and overall reactivity were poor. Improved results were obtained with calcium/zirconia sorbents. Future work will focus on development of more active, more attrition-resistant materials.

## References

1. DOE Report No. DOE/SC/FE-1, "Carbon Sequestration Research and Development" December 1999.
2. Kane, R.L.; and D.E. Klein, Chemical Engineering Progress, pp. 44-52. June 2001.
3. Herzog, H.; Environmental Science and Technology, **35**:7, pp. 148A-153A, April 1, 2001.
4. Rao, A.B.; and E.S. Rubin, Environmental Science & Technology, **36**:20, pp. 4467-4475, October 2002.
5. Herzog, H.; Drake, E.; and E. Adams, CO<sub>2</sub> Capture, Reuse, and Storage Technologies for Mitigating Global Climate Change, Final Report DOE Contract No. DE-AF22-96PC01257, January 1997.
6. Gupta, H.; and L.S. Fan, Industrial & Engineering Chemistry Research, **41**:16, pp. 4035-4042, August, 2002.

# SIMULATION OF RATE-BASED THEORETICAL MODEL FOR CO<sub>2</sub> CAPTURE: MASS TRANSFER AND HYDRODYNAMIC ASPECTS

Adisorn Aroonwilas and Amornvadee Veawab

Faculty of Engineering, University of Regina,  
Saskatchewan, Canada S4S 0A2

## Introduction

Carbon dioxide (CO<sub>2</sub>) absorption process is an immediate capturing technique suitable for the high-volume waste gas streams from coal-fired power plants. However, the overall cost of this process is relatively high. One reason for this high cost is the use of rule-of-thumb or approximation technique for the process design. Customarily, the absorption column is designed using the lumped mass-transfer and hydrodynamic parameters that are simply assumed to be constant over the entire length of the column, leading to an unnecessary oversized unit. With the advent of the environmental crisis and the economic constraint, the approximation is no longer applicable to process design. It is therefore necessary to obtain a better understanding of the actual phenomena taking place in this particular system so that a more rigorous and accurate column design technique can be developed. This paper presents a mechanistic concept for a rigorous absorber design that describes mass-transfer and hydrodynamic behavior within the CO<sub>2</sub> absorption columns fitted with structured packings.

## Mechanistic Concept

The development of mechanistic concept was based on an integration of various theoretical models that aim to determine the distribution pattern of the flowing liquid inside the packing element, effective interfacial area, mass-transfer coefficients and other information such as thermodynamic contributions (vapor-liquid equilibrium-VLE). Each model is briefly described below. Complete details can be found in the thesis of Aroonwilas [1].

## Liquid Distribution Model

The liquid distribution model (LDM) was developed in order to evaluate the distribution features of irrigating liquid, at different locations inside the packing element, during the operation of the absorption columns. The model is composed of two major components; i) a distribution structure representing a network of all possible flow-paths (connecting between packing intersections) through which the liquid can travel within the packing element and ii) a distribution intensity that indicates the quantity of irrigating liquid in each path (liquid rivulet). The liquid distribution features were generated by taking into account the details of the packing sheet arrangement and perforation, including dimensions, coordinates and patterns of the opening space on the packing sheets.

## Effective Interfacial Area Model

After the flow rates of liquid rivulets in all flow-paths were assigned by the liquid distribution model, the effective area for mass-transfer process was then evaluated from the calculated liquid rivulet dimensions (width and thickness). The calculations were based on the Shi and Marsmann's equations [2]. Such equations take into account physical properties of the associated liquid solution, including density, viscosity, surface tension and contact angle.

## Mass-Transfer Coefficient Model

The determination of absorption performance directly involves coefficients of mass-transfer across the gas-liquid boundary. The overall mass-transfer coefficient in the absorption system associated

with chemical reactions can be determined from two-film theory. The liquid-phase mass-transfer coefficient ( $k_L^\circ$ ) can be estimated from Penetration Theory as shown below.

$$k_L^\circ = 2\sqrt{\frac{D_{A,L}}{\pi t}} \quad (1)$$

where  $D_{A,L}$  and  $t$  are liquid-phase diffusivity coefficient of component  $A$  and gas-liquid contact time, respectively. The gas-phase mass-transfer coefficient ( $k_G$ ) can be estimated from equation 2 [3].

$$Sh_G = 0.0338(Re_G)^{0.8}(Sc_G)^{0.333} \quad (2)$$

where  $Sh_G$ ,  $Re_G$  and  $Sc_G$  represent Sherwood number, Reynolds number and Schmidt number, respectively. The enhancement factor due to chemical reactions can be evaluated by using the relationships proposed by DeCoursey & Thring [4].

## Thermodynamic Model

The vapor-liquid equilibrium (VLE) behavior of the CO<sub>2</sub> absorption system is another important element of the mechanistic model presented in this study. The equilibrium establishes concentration gradient between the gas and liquid phases, driving the mass-transfer process to proceed. An understanding of the equilibrium behavior is particularly essential for CO<sub>2</sub> absorption using aqueous alkanolamine solutions. In this work, the equilibrium behavior of the CO<sub>2</sub>-MEA system was evaluated by using the electrolyte NRTL model proposed by Austgen and colleagues [5]. The model can provide the necessary thermodynamic information, including the speciation (concentrations of different ionic species and molecules) in the CO<sub>2</sub> absorption system. This means that the concentration of free CO<sub>2</sub> in the bulk liquid can be estimated.

## MODEL SIMULATION

A Fortran-90 computer program was written for the mechanistic concept in order to simulate the CO<sub>2</sub> absorption performance of columns packed with structured packings. The simulation was based on the theoretical column design procedure for adiabatic gas absorption with chemical reaction. The procedure accounted for heats of absorption, solvent evaporation and condensation, chemical reactions in the liquid phase, and heat-and mass-transfer resistance in both gas and liquid phases.

The simulation of the absorption column was achieved by dividing the column or packing height into a number of sections with height  $dz$ . Each of these sections was treated as a non-equilibrium (or rate-based) discrete stage, which was governed by the material and energy equations.

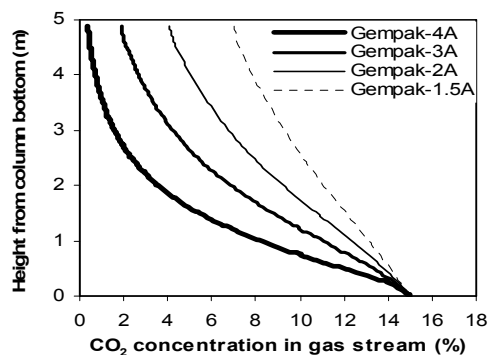
Each run of computer simulation gave essential information for the design of absorption system. These include concentration of CO<sub>2</sub> in the gas-phase, concentration of reactive species in the liquid-phase, system temperature, mass-transfer coefficients and the effective interfacial area at different axial positions along the absorption column. The simulation results were generally presented as plots against the column height to show the extent of the variation in process parameters at different column positions. The simulation also provided the plots, which represent quality of the liquid distribution across the cross-section of the column.

The model was successfully verified by comparing the simulated and experimental CO<sub>2</sub> concentration profiles for CO<sub>2</sub>-MEA system under two extreme conditions, depending upon the

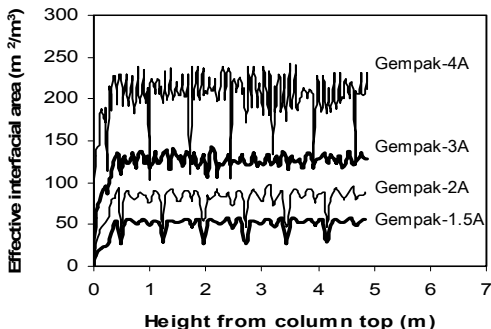
significance of thermodynamics contribution in controlling the mass-transfer phenomena.

## SIMULATION RESULTS

The simulation was carried out for the absorbers containing stainless-steel structured packings with different specific surface area ranging from 170 to 500  $\text{m}^2/\text{m}^3$ , i.e. Gempak-1.5A, Gempak-2A, Gempak-3A, and Gempak-4A. The simulation was based on 15%  $\text{CO}_2$  in feed gas and 1 m/s gas velocity. Figure 1-(a) shows the concentration profiles for the absorbers with the packing height of 5 m. The Gempak-4A having the surface area of 500  $\text{m}^2/\text{m}^3$  provided the highest recovery performance (98%), whereas the Gempak-1.5A having the area of 170  $\text{m}^2/\text{m}^3$  gave the lowest value of 57%. The Gempak-3A and -2A provided the recovery values in between the two extremes, i.e. 89% and 76%, respectively. The difference in the recovery performance of these packings is due to the difference in the effective interfacial area shown in Figure 1-(b).



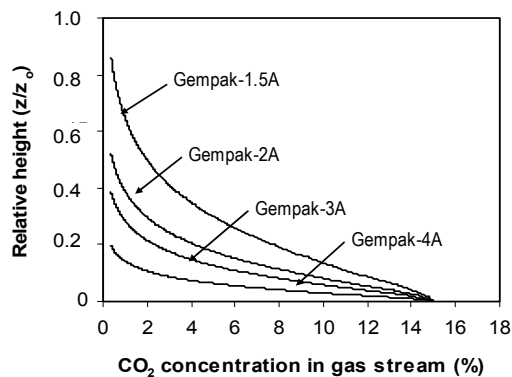
(a)



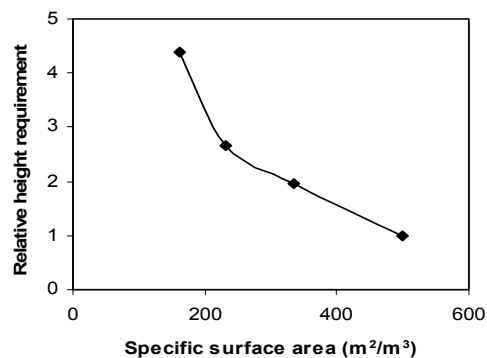
(b)

**Figure 1.**  $\text{CO}_2$  recovery performance of different structured packings.

Figure 2-(a) illustrates the  $\text{CO}_2$  concentration profiles for the absorbers used to recover 1075  $\text{kg CO}_2/\text{m}^2\text{-hr}$ . Based on this information, the relationship between the specific surface area of packing and the packing height requirement for a given recovery target can be plotted in Figure 2-(b). The required packing height increases proportionally as the packing surface area decreases from 500 to 233  $\text{m}^2/\text{m}^3$ . However, the height requirement increases substantially when the surface area is reduced to 170  $\text{m}^2/\text{m}^3$ .



(a)



(b)

**Figure 2.** Height requirement for different structured packings.

## Acknowledgement

Financial support from the Natural Sciences and Engineering Research Council of Canada (NSERC) is gratefully acknowledged.

## References

1. Aroonwilas, A., Ph.D. Thesis: University of Regina, Canada, 2001.
2. Shi, M. G.; Mersmann, A., *German Chemical Engineering*, **1985**, 8, 87-96.
3. Bravo, J. L.; Rocha, J. A.; Fair, J. R., *Hydrocarbon Processing* **1985**, 64, 91-95.
4. DeCoursey, W. J.; Thring, R. W., *Chemical Engineering Science*, **1989**, 44, 1715-1721.
5. Austgen, D. M.; Rochelle, G. T.; Peng, X. and Chen, C., *Industrial & Engineering Chemistry Research*, **1989**, 28, 1060-1073.